Integrated Master in Chemical Engineering

Energy efficient adsorption processes for environmental applications

Master's Thesis

by

Luís Alberto Macedo e Rocha

SINTEF – Materials and Chemistry

FEUP Supervisor: **Prof. Adélio Mendes**

SINTEF Supervisor: **Dr. Carlos Grande**

Departamento de Engenharia Química

July 2015

Acknowledgments

I would like to show my sincere gratitude to my supervisors Dr. Carlos Grande at SINTEF and Professor Adélio Mendes at FEUP, for allowing me to take part in this project and for all their help and availability during this internship. Thanks to them I was able to learn a lot during these 5 months and interact with an exciting work.

To Mahdi Abdollahzadeh I would like to acknowledge the help and suggestions given during the development of the mathematical model and numerical methods.

To my family and friends I would like to express my gratitude for all the support, motivation and friendship throughout all the work on this thesis.

The support of the Research Council of Norway through the CLIMIT program by the SINTERCAP project (233818). This publication has been produced with support from the BIGCCS Centre, performed under the Norwegian research program Centres for Environment-friendly Energy Research (FME). The author acknowledges the following partners for their contributions: ConocoPhillips, Gassco, Shell, Statoil, TOTAL, GDF SUEZ and the Research Council of Norway (193816/S60).

Abstract

CH_4/CO_2 separation is relevant for the treatment of natural gas. Among the different technologies employed nowadays to ensure that separation, adsorption has become more important and has plenty of potential for improvement. In this work, the carbon molecular sieve KP – 407 was studied for the separation of a stream of 90 % methane and 10 % carbon dioxide. The equilibrium and kinetic properties of the adsorbent were studied based on adsorption equilibrium isotherms, uptake curves and breakthrough curves.

The adsorption isotherms of carbon dioxide and methane were measured at 298 and 343 K and fitted with the multisite Langmuir model; the adsorbent displays a slightly greater affinity towards CO_2 compared with methane. The uptake curves were analysed to determine the kinetic properties of the two components; carbon dioxide diffuses much more rapidly through the micropores of the adsorbent than methane. Methane presents an additional constriction at the pore mouth having an important contribution towards the overall resistance to CH_4 diffusion.

Breakthrough curve experiments were performed at pressures from 5 to 70 bar in order to simulate the high pressure conditions of natural gas handling. A comprehensive phenomenological model to describe these experiments was detailed and was used to simulate the breakthrough curves. These experiments suggest that further work is necessary since the regeneration of the column during the fixed bed experiments was not complete.

Therefore, this work provides the description and implementation of a sophisticated mathematical model for the simulation of a fixed bed adsorption column and the analysis of experiments on adsorption equilibrium, kinetics and breakthrough curves. In addition, it presents the study of a new adsorbent and its behaviour at pressures as high as 70 bar.

Keywords: adsorption, natural gas, equilibrium, kinetics, breakthrough curves, modelling.

Resumo

A separação CH_4/CO_2 é relevante no tratamento de gás natural. Entre as diferentes tecnologias empregues nos dias de hoje para assegurar essa separação, a adsorção tem-se tornado uma das mais importantes e com maior potencial de evolução. Neste trabalho, a peneira molecular de carbono KP – 407 foi estudada para a separação de uma corrente de 90 % de metano e 1 0% de dióxido de carbono. O equilíbrio e cinética desses componentes neste adsorvente foram estudados, juntamente com experiências de curvas de rutura a diferentes pressões.

As isotérmicas de adsorção foram medidas a 298 e 343 K, tendo sido ajustadas com o modelo multisite Langmuir. O adsorvente demonstrou uma maior afinidade para com o CO_2, apesar da baixa seletividade de equilíbrio. As curvas de *uptake* foram analisadas para determinar os parâmetros cinéticos dos componentes. O dióxido de carbono difunde-se através dos microporos muito mais rapidamente que o metano, sendo que a constrição na entrada dos poros tem uma contribuição importante na resistência à difusão deste componente.

Experiências de curvas de rutura foram realizadas a pressões desde 5 até 70 bar, de modo a simular as condições de alta pressão no manuseamento de gás natural. Um modelo matemático para descrever estas experiências é detalhado e utilizado em simulações. Estas experiências sugerem que trabalho adicional é necessário para descrever e simular a cinética dos compostos envolvidos nesta separação.

Assim, este trabalho apresenta a descrição de um detalhado e sofisticado modelo matemático para a descrição de curvas de rutura juntamente com experiências de equilíbrio, cinética e leito fixo. As propriedades de um novo adsorvente são desta forma apresentadas a pressões até 70 bar.

Palavras chave: adsorção, gás natural, equilíbrio, cinética, curvas de rutura, modelização.

Official Statement

I declare, under honor commitment, that the presente work is original and that every non original contribution was properly referred, by identifying its origin.

Luís Alberto Macedo e Rocha

Table of Contents

List of Figures

List of Tables

Glossary

a_i	Number of neighbouring sites that can be occupied by and adsorbate particle in the multisite Langmuir model	-
a_p	Pellet specific area	m^{-1}
Bi	Biot number of component *i*	-
c_i	Molar concentration of component *i* in the fluid phase	$mol \cdot m^{-3}$
$\bar{c}_i$	Average concentration of component *i* in the macropores	$mol \cdot m^{-3}$
C_T	Total concentration in the fluid phase	$mol \cdot m^{-3}$
C_p	Molar constant pressure specific heat of the gas mixture	$J \cdot mol^{-1} \cdot K^{-1}$
C_{ps}	Constant pressure specific heat of the adsorbent	$J \cdot kg^{-1} \cdot K^{-1}$
C_{pw}	Specific heat of the column wall	$J \cdot kg^{-1} \cdot K^{-1}$
$C_{v,i}$	Molar constant volumetric specific heat of component *i*	$J \cdot mol^{-1} \cdot K^{-1}$
$C_{v,ads,i}$	Molar constant volumetric specific heat of component *i* adsorbed	$J \cdot mol^{-1} \cdot K^{-1}$
D_{ax}	Axial dispersion coefficient	$m^2 \cdot s^{-1}$
D_c	Micropore diffusion coefficient	$m^2 \cdot s^{-1}$
D_p	Macropore diffusion coefficient	$m^2 \cdot s^{-1}$
h_f	Film heat transfer coefficient between gas and solid	$W \cdot m^{-2} \cdot K^{-1}$
h_w	Film heat transfer coefficient between gas and the wall	$W \cdot m^{-2} \cdot K^{-1}$
K_i	Adsorption constant	bar^{-1}
$K_{0,i}$	Adsorption constant at infinite temperature	bar^{-1}
$k_{f,i}$	Film mass transfer coefficient of component *i*	$m \cdot s^{-1}$
$k_{p,i}$	Macropore diffusion constant of component *i*	s^{-1}
$k_{\mu,i}$	Micropore diffusion constant of component *i*	s^{-1}
Pe	Péclet number	-
P_i	Partial pressure of component *i*	Pa
P_T	Total pressure	Pa
$q_{m,i}$	Maximum adsorption capacity	$mol \cdot kg^{-1}$
$q_{s,i}$	Adsorbed phase concentration in equilibrium with the gas inside the particle for component *i*	$mol \cdot kg^{-1}$
$\bar{q}_i$	Average adsorbed concentration for component *I* in the pellet	$mol \cdot kg^{-1}$
$\Re$	Ideal gas constant	$J \cdot mol^{-1} \cdot K^{-1}$
r_c	Crystal radius	m
r_p	Pore radius	m

r_w	Radius of the wall	m
t	time	s
T_g	Gas temperature	K
T_s	Solid temperature	K
T_w	Wall temperature	K
T_∞	Ambient temperature	K
U	Overall heat transfer coefficient	$W \cdot m^{-2} \cdot K^{-1}$
u	Superficial gas velocity	$m \cdot s^{-1}$
z	Axial distance along the column	M

Greek letters

α_w	Ratio of the internal surface area to the volume of the column wall	m^{-1}
α_{wl}	Ratio of the log mean surface to the volume of the column wall	m^{-1}
$-\Delta H_i$	Isosteric heat of adsorption of *I* component	$J \cdot mol^{-1}$
ε_b	Porosity of the column	-
ε_p	Porosity of the pellet	-
λ	Axial heat dispersion coefficient	$W \cdot m^{-2} \cdot K^{-1}$
μ_g	Gas viscosity	Pa·s
ρ_g	Gas density	$kg \cdot m^{-3}$
ρ_p	Pellet density	$kg \cdot m^{-3}$
ρ_w	Column wall density	$kg \cdot m^{-3}$

List of Acronyms

BPR	Back-pressure regulator
MFC	Mass flow controller
MS	Mass spectrometer
PSA	Pressure swing adsorption

1 Introduction

1.1 Motivation and Relevance

The production of sufficient energy with economic viability and environmental sustainability is one of the main concerns nowadays [1]. Given its importance as a fuel and as a source of hydrocarbons for petrochemical feed stocks, the use of natural gas must therefore follow the aforementioned requirements. One of the main issues regarding the handling and treatment of natural gas is the separation of impurities such as carbon dioxide from the main constituent of the gas, methane. The removal of CO_2 is a very important step to ensure the pipeline specifications of natural gas, since its presence in the stream reduce their calorific value and make them acidic and corrosive, reducing the possibilities of gas compression and affecting its transport.

Numerous methods have been studied and implemented for the separation of CO_2 from CH_4, such as absorption [1],[2],[3], cryogenic distillation [1],[3] and membrane processes [1], [2], [4]. Adsorption technologies such as pressure swing adsorption (PSA) and temperature swing adsorption (TSA) have recently started to be applied to methane purification from natural gas and have a great potential to expand its utilization [1], [5], [6].

One of the most important aspects that affect the behaviour of adsorption technologies is the adsorbent employed for the separation. The adsorbent should exhibit appropriate selectivity, capacity, service life and ease of regeneration [6], [7]. The diffusion properties of the various gases through the adsorbent are also relevant, since adsorption processes for CO_2/CH_4 separation are often kinetically controlled. It is thus very important to examine the equilibrium and kinetic properties of the adsorbents used.

In addition, natural gas and methane are often stored and handled at very high pressures [8]. While the behaviour and characteristics of adsorption processes for methane purification are well known at low pressures [5], it is relevant to know how these properties are affected when the pressure is higher.

Another important feature in the study of adsorption processes is process simulation. This allows for a better understanding of the phenomena involved, and the optimization of the variables involved in the process. An effective simulation is based on the creation of accurate mathematical models of the system, as well as the use of powerful numerical methods or commercial software programs to solve the equations.

In this work, the equilibrium and kinetic properties of a new adsorbent were studied, and this material was used in breakthrough curve experiments under pressures up to 70 bar. A

mathematical model of the system is described and was used to simulate the results. The mass, energy and momentum balances are presented, together with the necessary correlations to estimate the transport parameters. The numerical solution of the partial differential equations that define the system was initially studied in Python and the simulations were later performed with gPROMS.

All the experiments mentioned in this report were performed at SINTEF before the author's involvement in the project. Therefore, the work involved the treatment and interpretation of all the raw data.

1.2 Outline

This work is divided into 5 main parts.

The first chapter described the motivation and relevance of this study.

The second chapter is the state of the art, presenting a brief description of the current adsorption technology, including the carbon molecular sieves and the fundamentals of PSA processes.

The third chapter presents the technical description of this work. It contains the description of the experimental and theoretical elements of the study of the equilibrium and kinetic properties of the adsorbent. The mathematical model used in the simulations is also presented.

The fourth chapter is dedicated to the presentation of the results obtained and discussion. Adsorption isotherms and the results of uptake kinetics experiments are shown, as well as the experimental and simulated breakthrough curves.

Finally, the fifth chapter includes the main conclusions of this thesis.

2 State of the Art

2.1 Carbon molecular sieves

Activated carbon is a predominantly amorphous solid that has an extraordinarily large internal surface area and pore volume, and thus a large capacity for adsorbing chemicals from gases and liquids. The structure of activated carbon can be described as a twisted network of defective carbon layer planes, cross-linked by aliphatic bridging groups. The main characteristics of an activated carbon, the surface area, dimensions and distribution of the pores depend on the precursor and the conditions of carbonization and activation [9].

Molecular sieves are materials with discrete pore structures that can discriminate between molecules on the basis of size. Therefore, carbon molecular sieves (CMS) are a special class of activated carbons. Activated carbons will mostly separate molecules according to different adsorption capacities of different species, while CMS operate based on different rates of adsorption [9].

All carbon materials are prepared from carbonaceous matter such as coal, wood, polymers, among others. Coal is the most common starting material and is turned into activated carbon by a two-step process of carbonization and activation. The first step converts the coal from thermoplastic to thermosetting and the second involves opening up closed porosity and the enlargement of existing pores [9].

The main use of carbon molecular sieves is processes of separation and purification of gases, namely the separation of nitrogen from oxygen, hydrogen from methane or hydrogen from ammonia [9]. CMS has also been found useful in catalysis processes [9].

2.2 Pressure swing adsorption

In an adsorption process, different molecules have different levels of interaction with the adsorbent, either in the amount that is adsorbed in the equilibrium or how fast the molecules diffuse through the pores of the material. From these differences in behaviour, it is eventually possible to separate different components. An adsorption column is usually filled with the adsorbent in fixed beds. As the feed stream goes through the column, some components will be more adsorbed than others. The less adsorbed component will break through the column faster than the others, therefore, in order to achieve separation, the feed should be stopped and the adsorbent regenerated. Since the adsorption equilibrium is dependent on the operating conditions (composition, temperature and pressure) by changing one of these parameters it is possible to regenerate the adsorbent. A pressure swing adsorption process happens when the

pressure is reduced to regenerate the adsorbent and increased for the feed, making the pressure "swing" [6].

The behaviour of a PSA unit is dependent on two main areas: the adsorbent chosen for the separation and the strategy employed to regenerate the adsorbent. Thus, the main areas of research in PSA units include material science for the creation of new and more effective adsorbents and engineering to develop novel methods to regenerate them.

If a PSA unit consists of a single adsorption column, the separation process will regularly be interrupted to regenerate the adsorbent. In order to achieve a continuous process, a two-column PSA unit was presented by Charles Skarstrom [10]. With two columns, it is possible to have a column regenerating while the other is being fed. The original system proposed by Skarstrom included four steps: feed, blowdown, purge and pressurization. However, ever since is work was published numerous changes have been suggested, including the introduction of additional steps or use of multiple columns [6], [11]. The use of vacuum has also been studied, to cause a more extreme regeneration in a process called vacuum pressure swing adsorption. The invention of more complex PSA systems has also increased the challenge of optimizing the cyclic strategies of the unit to improve its performance. Modelling has consequently become more important and several commercial programs such as ASPEN, COMSOL and gPROMS have been used in this context.

While being an established technology in the fields of air separation, drying and hydrogen purification, PSA still has not become a fully successful technique in other fields, due to its complexity. Improvements in the areas of materials science and process engineering will seek to spread the applications of this technology.

3 Mathematical modelling

Adsorption is defined as the spontaneous attraction phenomenon experienced by a molecule in a fluid phase when close to the surface of a solid. These particles form a thin layer called *adsorbate* on the surface of a solid named *adsorbent*. This process is exothermic and its driving force is the reduction in interfacial surface tension between the fluid being adsorbed and the solid adsorbent [6], [12], [13].

The study of adsorption phenomena seeks to describe the equilibrium and kinetics of single and multicomponent systems.

3.1 Adsorption equilibrium

Adsorption equilibrium is described through the medium of adsorption isotherms. An isotherm represents the amount of a certain adsorbed component as a function of the amount of that component present in the fluid phase. Since temperature affects adsorption equilibrium, a particular isotherm is valid for a specific temperature. A large number of models have been proposed as adsorption isotherms [14]. The choice of which model to use to fit experimental data will be related to the physical assumptions made in the model, the quality of the data fit and the mathematical complexity of the isotherm (some isotherms may impose longer computational times when used in breakthrough curves simulations). Below are described some of the most common adsorption isotherms.

Langmuir model

The Langmuir model [13] is the simplest and most frequently used model to describe monolayer adsorption. It is based on the following assumptions:

1. The adsorbent has a certain fixed number of well-defined localized sites;
2. Each adsorption site accommodates only one adsorbate molecule;
3. Adsorption energy is constant on all sites;
4. There is no lateral energetic interaction between molecules adsorbed on neighbouring sites.

The model is described by equation (3.1):

$$q_s = \frac{q_m K c}{1 + Kc} \tag{3.1}$$

where q_s is the adsorbate concentration in the solid phase, q_m is the saturation capacity of the adsorbate, c is the concentration of the adsorbate in the fluid phase and K is the adsorption

constant. The dependence of the adsorption constant with temperature is given by the Van't Hoff equation:

$$K = K_0 e^{-\Delta H/\Re T} \tag{3.2}$$

where K_0 the adsorption constant at infinite temperature, $-\Delta H$ is the heat of adsorption, $\Re$ is the universal gas constant and T is the temperature of the system.

When two or more components are present in the system, these will compete for the limited number of adsorption sites. Therefore, a mere single component isotherm will not describe the process accurately. It is then necessary to define multicomponent extensions to the known isotherms. The multicomponent Langmuir isotherm is given by equation (3.3):

$$q_{s,i} = \frac{q_{m,i} K_i c_i}{1 + \sum K_i c_i} \tag{3.3}$$

Freundlich model

Unlike the Langmuir model, which is based on theoretical assumptions, the Freundlich isotherm is an entirely empirical isotherm. It is therefore used as an alternative to isotherms with a theoretical background. The isotherm is given by equation (3.4):

$$q_s = K c^{\frac{1}{n}} \tag{3.4}$$

where K and n are temperature dependent constants.

Multisite Langmuir model

This model is an extension of the Langmuir model for single component and multicomponent equilibrium on microporous, homogeneous adsorbents that takes into account the variation of adsorbate size. It assumes that the adsorbent has a limited number of adsorption sites and that the adsorbate particles occupy a certain number of these sites. The model is described by equation (3.5):

$$\frac{q}{q_m} = KP\left(1 - \frac{q}{q_m}\right)^a \tag{3.5}$$

where a represents the number of neighbouring sites that can be occupied by an adsorbate particle. The remaining parameters have the same significance as in the Langmuir isotherm. In fact, the multisite Langmuir isotherm corresponds to the Langmuir isotherm when $a = 1$.

The multicomponent extension of the model is given by equation (3.6):

$$\frac{q_i}{q_{m,i}} = K_i P_i \left(1 - \sum_{i=1}^{n} \frac{q_i}{q_{m,i}}\right)^{a_i} \tag{3.6}$$

Given the assumptions described above about the fixed number of sites on the adsorbent, the following relation must be verified in multicomponent systems to ensure thermodynamic consistency:

$$q_{m,i}.a_i = constant$$

Toth model

The Toth model is another empirical model designed to provide an improved data fit when compared to the more traditional isotherms described above. Consequently, it has a higher number of parameters. The isotherm is described by equation (3.7):

$$q_s = \frac{Kc}{[1+(Kc)^n]^{1/n}} \tag{3.7}$$

where K is calculated from equation (3.2) and n is given by:

$$n = A + BT \tag{3.8}$$

The Toth isotherm is very effective at fitting experimental data but, just like the Freundlich isotherm, lacks any theoretical meaning.

3.2 Adsorption kinetics

Adsorption columns and PSA units are dynamic separation processes which means that it is very important to know the velocity of the gases through the porous structure of the adsorbent. This is particularly important when the resistances to diffusion are very different between the various components being separated, making the process kinetically controlled.

Experiments are carried out to determine if the studied separation is kinetically controlled and to obtain estimates of the kinetic properties of the compounds, namely the micropore diffusion constants. When measuring the adsorption equilibrium data, the approach to equilibrium of the first point was used to estimate the diffusion kinetics of pure gases. In such a case, the system behaves as a batch system with a finite volume.

Carbon molecular sieves such as the one used in this work are bidisperse adsorbents, which means that its pore structure is composed of macropores branched with micropores. As a consequence, the controlling mechanism may be diffusion in the macropores, diffusion in the micropores or both. For gas adsorption, the controlling resistance is almost always located in the micropores. However, in this case, the constriction present in the pore mouths may share or even control the diffusion process [18]. In order to describe the diffusion in micropores where the effect of the constriction at the mouth is important, a dual-resistance model may be used, with a term for the barrier mass transfer at the mouth and another for the micropore resistance. The

mathematical model presented below was used to describe this process. The model assumes that the process is isothermal and that the isotherm is quite linear in the very low pressure range.

The mass balance in the gravimetric cell is given by equation (3.9):

$$C(t) = \left[C_0 - \frac{m_s}{V_c}\langle\bar{q}(t)\rangle\right] \tag{3.9}$$

Average amount adsorbed in the extrudates:

$$\langle\bar{q}\rangle = \frac{2}{r_p^2}\int_0^{r_p}\bar{q}RdR \tag{3.10}$$

Mass balance in the extrudates, with initial and boundary conditions:

$$\varepsilon_p\frac{\partial C_p}{\partial t} + \rho_p\frac{\partial\bar{q}}{\partial t} = \frac{\varepsilon_p D_p}{R}\frac{\partial}{\partial R}\left(R\frac{\partial C_p}{\partial R}\right) \tag{3.11}$$

$$\varepsilon_p D_p\frac{\partial C}{\partial R}_{(t,r_p)} = k_f\left(C - C_{p(t,r_p)}\right) \tag{3.12}$$

$$\frac{\partial C_p}{\partial R}_{(0,t)} = 0 \tag{3.13}$$

$$C_{(R,t=0)} = 0 \tag{3.14}$$

Average amount adsorbed in the micropores:

$$\bar{q} = \frac{3}{r_c^3}\int_0^{r_c} qr^2dr \tag{3.15}$$

Fick law of diffusion in the micropores, with initial and boundary conditions:

$$\frac{\partial q}{\partial t} = \frac{1}{r^2}D_\mu^\infty\frac{\partial}{\partial r}\left[r^2\frac{\partial q}{\partial r}\right] \tag{3.16}$$

$$\frac{3}{r_c}D_\mu^\infty\frac{\partial q}{\partial r}_{r=r_\mu} = k_b(q^* - q)_{r=r_\mu} \tag{3.17}$$

$$\frac{\partial q}{\partial r}_{(0,t)} = 0 \tag{3.18}$$

$$q_{(r,t=0)} = 0 \tag{3.19}$$

The LDF constant is calculated with equation (3.20):

$$k_{\mu,i} = \frac{1}{\frac{1}{k_{b,i}} + \frac{r_c^2}{15D_{c,i}}} \tag{3.20}$$

In the particular case when the constriction at the pore mouth can be neglected, a simplified model can be used. The following expression can be derived to describe the kinetics of adsorption for long times [12]:

$$\frac{q}{q_{eq}} = 1 - 6\sum_{n=1}^{\infty} \frac{\exp\left(-p_n^2 K_{\mu,i} t\right)}{9\frac{\Lambda}{1-\Lambda} + (1-\Lambda)p_n^2} \tag{3.21}$$

where q is the amount adsorbent as it changes with time, q_{eq} is the amount adsorbed when equilibrium is reached and $K_{\mu,i}$ is the micropore diffusion constant defined by:

$$k_{\mu,i} = \frac{15 D_{c,i}}{r_c^2} \tag{3.22}$$

Λ is the factor describing the variation of the concentration with time, given by equation (3.23):

$$\Lambda = \frac{C_{ini} - C_{eq}}{C_{ini}} \tag{3.23}$$

The variable p_n refers to the roots of equation (3.24):

$$\tan(p_n) = \frac{3p_n}{3 + \left(\frac{1}{\Lambda} - 1\right)p_n^2} \tag{3.24}$$

To achieve an acceptable description of the diffusion in short times, at least the first 40 roots of the equation are required [17].

The results obtained from the diffusion experiments will clarify the influence of the micropore mouth constriction in the overall diffusion process.

3.3 Fixed-bed adsorption model

A mathematical model was developed to describe the behaviour of a fixed-bed adsorption column [19]. This model was based on the following assumptions:

- Mass, velocity and temperature gradients in the radial direction are negligible;
- The flow pattern is described by the axially dispersed plug flow model;
- Uniform adsorbent properties in the column;
- Constant cross section area.

The complete model consists of coupled partial differential equations and algebraic equations that need to be solved in time and space. The number of equations required to properly describe the system depends on its characteristics as well as the intended accuracy of the simulations. Therefore, in order to have a better understanding of the dynamics of the adsorption process of multicomponent mixtures in a fixed bed, several models were studied.

3.3.1 Mass balance equations

Component mass balance

Since the flow pattern is given by the axially dispersed plug flow model, it is relevant to properly understand what each term in the mathematical equation represents. This model is described by equation (3.25):

$$\varepsilon_b \frac{\partial c_i}{\partial t} = -\varepsilon_b \frac{\partial (u_i c_i)}{\partial z} + \frac{\partial}{\partial z}\left(\varepsilon_b D_{ax} C_T \frac{\partial y_i}{\partial z}\right) - N_i \tag{3.25}$$

where c_i is the concentration of component *i* in the fluid phase, C_T is the total concentration in the fluid phase, y_i is the molar fraction of component *i*, u_i is the interstitial velocity, D_{ax} is the axial dispersion coefficient, ε_b is the bed porosity, t is time and z is the position along the column. The meaning of the different terms in the equation is given in Table 3.1:

Table 3.1 – Meaning of the main terms present the in mass balance equations.

Mass balance term	Name	Description
$\varepsilon_b \frac{\partial c_i}{\partial t}$	Accumulation term	Describes how the fluid phase concentration of component i varies with time.
$\varepsilon_b \frac{\partial (u_i c_i)}{\partial z}$	Convective term	Describes the variation of the fluid phase concentration as it passes through the column
$\frac{\partial}{\partial z}\left(\varepsilon_b D_{ax} C_T \frac{\partial y_i}{\partial z}\right)$	Diffusive term	Describes the impact of axial dispersion on the concentration along the column
N_i	Molar flux of component i in the particle	Describes the flow of component i between the fluid phase and the particle; its exact form depends on the mass transfer mechanism between the two phases

The non-dimensional number that affects this equation is the Péclet number, defined by:

$$Pe = \frac{uL}{D_{ax}} \tag{3.26}$$

where *L* is the column length. This number indicates how important the effects of axial dispersion are in the system.

If there are no mass transfer resistances anywhere in the system, the molar flux of component *i* is given by equation (3.27). It adds a term representing the accumulation in the solid phase to the original equation.

$$N_i = (1 - \varepsilon_b)\rho_p \frac{\partial \bar{q}_i}{\partial t} \tag{3.27}$$

where ρ_p is the particle porosity and $\bar{q}_i$ the average concentration of component *i* in the adsorbent particle. In this case, the component mass balance and the appropriate adsorption isotherm are enough to mathematically predict the breakthrough curves of the column. However, if mass transfer resistances are present in the micropores, an additional equation is required to describe intraparticular mass transfer. The LDF model was used and is given by equation (3.28). The employment of the LDF model allows for a much reduced computational time without losing accuracy in the solution.

$$\frac{\partial \bar{q}_i}{\partial t} = k_{\mu,i}\left(q_{s,i} - \bar{q}_i\right) \tag{3.28}$$

where $q_{s,i}$ the concentration of the component *i* at the surface of the adsorbent and $k_{\mu,i}$ is the micropore diffusion constant, given by equation (3.22).

The complexity of the model can be increased further if the resistance to the diffusion in the macropores is considered important. In a similar manner as before, a term representing the accumulation in the macropores must be added to the component mass balance as well as a new equation describing the diffusion in the macropores is necessary. The molar flux is now given by equation (3.29):

$$N_i = (1 - \varepsilon_b)\left(\varepsilon_b \frac{\partial \bar{c}_i}{\partial t} + \rho_p \frac{\partial \bar{q}_i}{\partial t}\right) \tag{3.29}$$

where $\bar{c}_i$ is the concentration of component *i* in the macropores. Equation (3.30) describes the diffusion in the macropores:

$$\frac{\partial \bar{c}_i}{\partial t} = k_{p,i}\frac{Bi_i}{Bi_i + 1}(c_i - \bar{c}_i) - \frac{\rho_p}{\varepsilon_p}\frac{\partial \bar{q}_i}{\partial t} \tag{3.30}$$

where $k_{p,i}$ is the macropore diffusion constant and Bi_i is the mass Biot number. The macropore diffusion constant is given by:

$$k_{p,i} = \frac{15 D_{p,i}}{r_p^2} \tag{3.31}$$

where $D_{p,i}$ is the macropore diffusivity and r_p is the radius of the macropores. The mass Biot number is given by:

$$Bi_i = \frac{r_p\, k_{f,i}}{5\varepsilon_p D_{p,i}} \tag{3.32}$$

Finally, the diffusion in the film surrounding the pellet may be important as well. In that case, the molar flux assumes the form of equation (3.33):

$$N_i = (1-\varepsilon_b)\frac{a_p k_{f,i}}{(Bi-1)}(c_i - \bar{c}_i) \tag{3.33}$$

where $k_{f,i}$ is the external mass transfer coefficient for *i* component.

In order to simulate breakthrough curves with *n* components, *n* component mass balance equations together with the respective mass transfer equations are required. The process can also be described with *n* – 1 mass balance equations and an overall mass balance, obtained by applying a sum over all *n* mixture components as presented in equation (3.34):

$$\varepsilon_b \frac{\partial C_T}{\partial t} = -u_i \varepsilon_b \frac{\partial C_T}{\partial z} - \sum_{i=1}^{n} N_i \tag{3.34}$$

where C_T is the total concentration in the fluid phase.

3.3.2 Momentum balance equation

The balance of forces acting over the characteristic control volume is described by the Ergun equation, which considers the change of velocity and pressure drop along the column. The Ergun equation is given by equation (3.35):

$$\frac{\partial P}{\partial z} = -\frac{150\mu_g(1-\varepsilon_b)^2}{\varepsilon_b^3 d_p^2}u_i - \frac{1.75(1-\varepsilon_b)\rho_g}{\varepsilon_b^3 d_p}|u_i|u_i \tag{3.35}$$

where P is the total pressure, μ_g is the gas viscosity and ρ_g is the gas density. Given that the gas phase is assumed to follow the ideal gas law, the total pressure in the system is related to the total concentration through the ideal gas equation:

$$P_T = C_T \Re T \tag{3.36}$$

However, the ideal gas equation is only accurate in the low pressure range. For the mixture studied in this work, the gas density has been shown to deviate from the ideal trend at pressures above 30 bar and therefore employing that equation can introduce significant errors [22]. The Benedict-Webb-Rubin (BWR) equation of state was used to relate the pressure in the system with the total concentration in the fixed bed experiments with pressures higher than 30 bar.

$$P = \Re T C_T + \left(B_o \Re T - A_0 - \frac{C_0}{T^2}\right)C_T^2 + (b\Re T - a)C_T^3 + a\alpha C_T^6 + \frac{cC_T^3}{T^2}(1+\gamma C_T^2)e^{-\gamma C_T^2} \tag{3.37}$$

Table 3.2 – Expressions used to calculate the mixing parameters of the BWR equation.

$A_0 = \left[\sum_i y_i \left(A_{0,i}\right)^{1/2}\right]^2$	$a = \left[\sum_i y_i (a_i)^{1/3}\right]^3$
$B_0 = \sum_i y_i B_{0,i}$	$b = \left[\sum_i y_i (b_i)^{1/3}\right]^3$
$C_0 = \left[\sum_i y_i \left(C_{0,i}\right)^{1/2}\right]^2$	$c = \left[\sum_i y_i (c_i)^{1/3}\right]^3$
$\gamma = \left[\sum_i y_i (\gamma_i)^{1/2}\right]^2$	$\alpha = \left[\sum_i y_i (\alpha_i)^{1/3}\right]^3$

Table 3.3 – Constants of the BWR equation for CH_4 and CO_2.

	a	A_0	b	B_0	c	C_0	α	γ
CH_4	5	187.91	3.38×10^{-3}	4.26×10^{-2}	2.58×10^{5}	2.29×10^{6}	1.24×10^{-4}	6×10^{-3}
CO_2	13.86	277.30	7.21×10^{-3}	4.99×10^{-3}	1.51×10^{6}	1.40×10^{7}	8.47×10^{-5}	5.4×10^{-3}

3.3.3 Energy balance equations

Two different types of energy balance can be considered. If the three phases present in the column (gas, solid and column wall) are in thermal equilibrium (in other words, the heat transfer resistances are negligible between these three phases) then only one equation is necessary, named the "homogeneous energy balance". If, on the other hand, the heat transfer resistances are important, each phase requires an independent energy balance that are then coupled to each other through film energy transfer terms. This model is called "heterogeneous energy balance".

Heterogeneous energy balance

The gas phase energy balance is given by equation (3.38):

$$\varepsilon_b C_T C_{v,i} \frac{\partial T_g}{\partial t} = \frac{\partial}{\partial z}\left(\lambda \frac{\partial T_g}{\partial z}\right) - C_T C_{pg} \frac{\partial \left(u_i T_g\right)}{\partial z} + \varepsilon_b \Re T_g \frac{\partial C_T}{\partial t} - (1-\varepsilon_b) a_p h_f \left(T_g - T_s\right) - \frac{2h_w}{r_w}\left(T_g - T_w\right) \qquad (3.38)$$

where $C_{v,i}$is the molar constant volumetric heat of component *I*, λ is the axial heat dispersion coefficient, C_{pg} is the molar constant pressure specific heat of the gas mixture,

$\Re$ is the ideal gas constant, h_f is the film heat transfer coefficient between the gas and the solid phase, h_w is the film heat transfer coefficient between the gas phase and the column wall, r_w is the radius of the wall, T_g is the temperature of the gas, T_s is the temperature of the solid and T_w is the temperature of the wall.

The energy balance in the solid phase is given by equation (3.39):

$$(1-\varepsilon_b)\left\{\varepsilon_p \sum_{i=1}^{n} \bar{c}_i C_{v,i} + \rho_p \omega_c \sum_{i=1}^{n} \bar{q}_i C_{v,ads,i} + \rho_p C_{ps}\right\}\frac{\partial T_s}{\partial t}$$
$$= (1-\varepsilon_b)\varepsilon_p \Re T_s \frac{\partial \bar{c}}{\partial t} + \rho_b \omega_c \sum_{i=1}^{n}(-\Delta H_i)\frac{\partial \bar{q}_i}{\partial t} + (1-\varepsilon_b)a_p h_f\left(T_g - T_s\right) \quad (3.39)$$

where $C_{v,ads,i}$ is the molar constant volumetric specific heat of component *i* adsorbed, C_{ps} is the constant pressure specific heat of the adsorbent and ω_c is the crystal weight fraction of the pellet.

Finally, the column wall energy balance described by equation (3.40) completes the model.

$$\rho_w C_{pw}\frac{\partial T_w}{\partial t} = \alpha_w h_w\left(T_g - T_w\right) - \alpha_{wl} U(T_w - T_\infty) \quad (3.40)$$

where ρ_w is the wall density, C_{pw} is the specific heat of the adsorbent, U is the global external heat transfer coefficient, T_∞ is the ambient temperature, α_w is the ratio of the internal surface area to the volume of the column wall, given by:

$$\alpha_w = \frac{d_w}{e(d_w + e)} \quad (3.41)$$

where d_w is the column internal diameter and e is the thickness of the shell and α_{wl} is the ratio of the logarithmic mean surface area of the column shell to the volume of the column wall, given by:

$$\alpha_{wl} = \frac{1}{(d_w + e)\ln\left(\frac{d_w + e}{d_w}\right)} \quad (3.42)$$

Homogeneous energy balance

The homogeneous energy balance allows for a shorter computational time without affecting accuracy, if the heat transfer resistances are negligible. This model combines the gas, solid and wall balances into equation (3.43):

$$\left\{\varepsilon_b \sum_{i=1}^{n} c_i C_{pg,i} + (1-\varepsilon_b)\,\varepsilon_p \sum_{i=1}^{n} \bar{c}_i\, C_{pg,i} + (1-\varepsilon_b)\rho_p \omega_c \sum_{i=1}^{n} \bar{q}_i\, C_{pg,i} + (1-\varepsilon_b)\rho_p C_{ps} + \varepsilon_w \rho_w C_{pw}\right\}\frac{\partial T}{\partial t}$$

$$= \varepsilon_b \Re T \frac{\partial C_T}{\partial t} + \lambda \frac{d^2 T}{dz^2} + (1-\varepsilon_b)\varepsilon_p \Re T \frac{\partial \bar{c}}{\partial t} - u_i C_{pg,i} C_T \frac{\partial T}{\partial z} + \rho_b \omega_c \sum_{i=1}^{n} (-\Delta Hi) \frac{\partial \bar{q}_i}{\partial t}$$

$$- \varepsilon_w \alpha_{wl} U (T_w - T_\infty) \tag{3.43}$$

where ε_w is a geometric factor given by:

$$\varepsilon_w = \frac{4(d_w + e)e}{d_w^2} \tag{3.44}$$

Since this model assumes thermal equilibrium between the different phases:

$T = T_g = T_s = T_w$

The meaning of the main terms presented in these mathematical models is described in Table 3.4:

Table 3.4 – Meaning of the main terms present in the energy balance

Energy balance term	Name	Description
$\varepsilon_b C_T C_{v,i} \frac{\partial T_g}{\partial t}$	Fluid phase accumulation term	Describes stagnant fluid-phase energy accumulation over time.
$C_T C_{pg} \frac{\partial (u_i T_g)}{\partial z}$	Convective term	Describes the passage of energy through the column due to convection.
$\frac{\partial}{\partial z}\left(\lambda \frac{\partial T_g}{\partial z}\right)$	Diffusive term	Describes the transport of energy due to diffusion.
$\rho_b \omega_c \sum_{i=1}^{n} (-\Delta H_i) \frac{\partial \bar{q}_i}{\partial t}$	Generation term	Describes the generation of energy due to adsorption.
$(1 - \varepsilon_b)\left\{\varepsilon_p \sum_{i=1}^{n} \bar{c}_i C_{v,i} + \rho_p \omega_c \sum_{i=1}^{n} \bar{q}_i C_{v,ads,i} + \rho_p C_{ps}\right\}\frac{\partial T_s}{\partial t}$	Solid phase accumulation term	Describes the accumulation of energy in the solid phase over time.
$(1-\varepsilon_b) a_p h_f (T_g - T_s)$	Gas-solid exchange term	Describes how the fluid and solid phases exchange energy.

$\frac{2h_w}{r_w}(T_g - T_w)$	Gas-wall exchange term	Describes how the fluid phase and the column wall exchange energy.
$\alpha_{wl}U(T_w - T_\infty)$	Wall-Exterior exchange term	Describes how the column wall exchanges energy with the surrounding environment.

3.3.4 Transport parameters

The solution of the equations described above requires knowing the values of the various transport parameters that are present in them. These parameters were estimated with the correlations presented below.

The pore diffusivity, $D_{p,i}$, was approximated using the Bosanquet relationship, presented in equation (3.45):

$$\frac{1}{D_{p,i}} = \tau\left(\frac{1}{D_{m,i}} + \frac{1}{D_{k,i}}\right) \tag{3.45}$$

where τ is the tortuosity factor, $D_{m,i}$ is the molecular diffusion coefficient for the component *i* in the mixture and $D_{k,i}$ is the Knudsen diffusion.

The molecular diffusivity is estimated with equation (3.46).

$$D_{m,i} = \frac{1 - y_i}{\sum_{j=1, j\neq i}^{n} \frac{y_i}{D_{ij}}} \tag{3.46}$$

where D_{ij} are the molecular diffusivities of the components in the mixture.

The Knudsen diffusivity is given by expression (3.47):

$$D_{k,i} = 9.7 \times 10^{-9} r_p \sqrt{\frac{T}{M_i}} \tag{3.47}$$

where r_p is the pore radius in Å while the remaining variables are in SI units.

The axial dispersion parameters, $D_{ax,i}$ and λ were calculated with the following correlations:

$$\frac{\varepsilon_b D_{ax,i}}{D_{m,i}} = 20 + 0.5 Sc_i Re \tag{3.48}$$

$$\frac{\lambda}{k_g} = 7 + 0.5 Pr Re \tag{3.49}$$

where Sc_i is the Schmidt number for component *i*, Re is the Reynolds particle number, Pr is the Prandtl number and k_g is the thermal conductivity of the gas. These correlations are valid for values of the Reynolds number between 3 and 10000 with the dimensionless numbers involved being defined by the equations below:

$$Sc_i = \frac{\mu}{\rho D_{m,i}} \tag{3.50}$$

$$Re = \frac{\rho u d_p}{\mu} \tag{3.51}$$

$$Pr = \frac{C_{pg}\mu}{k_g} \tag{3.52}$$

The molar specific heat at constant pressure is calculated as presented in the equation:

$$C_{pg} = \sum_{i=1}^{n} y_i \, C_{pg,i} \tag{3.53}$$

where $C_{pg,i}$ are calculated with the following polynomials:

$$C_{pg,i} = \sum_{i=0}^{3} A_i T^i \tag{3.54}$$

where A_i are empirical constants for each component and T is the gas temperature. The molar specific heat at constant volume of the mixture and those of each component were calculated from the respective specific heats at constant pressure according to the ideal gas relationships:

$C_{vg,i} = C_{pg,i} - \Re$

$C_{vg} = C_{pg} - \Re$

The gas thermal conductivity of a single component is calculated as follows:

$$k_{g,i} = \left(C_{pg,i} + \frac{5}{4}\frac{\Re}{M_i}\right)\mu_i \tag{3.55}$$

and the one of the mixture with the following equation:

$$k_g = \sum_{i=1}^{n} \frac{y_i k_{g,i}}{\sum_{j=1}^{n} y_j \Phi_{ij}} \tag{3.56}$$

The film mass and heat transfer coefficients $k_{f,i}$ and h_f were estimated using the following correlations:

$$Sh_i = 2.0 + 1.1 Re^{0.6} Sc_i^{1/3} \tag{3.57}$$

$$Nu = 2.0 + 1.1 Re^{0.6} Pr^{1/3} \tag{3.58}$$

where Sh_i is the Sherwood number for component *i* and Nu is the Nusselt number. These dimensionless numbers are calculated as follows:

$$Sh_i = \frac{k_{f,i} d_p}{D_{m,i}} \tag{3.59}$$

$$Nu = \frac{h_f d_p}{k_g} \tag{3.60}$$

The global heat transfer coefficient can be obtained from equation (3.61):

$$\frac{1}{U} = \frac{1}{h_w} + \frac{e d_{in}}{\lambda_w d_{ln}} + \frac{d_{in}}{d_{ex} h_{ex}} \tag{3.61}$$

where e is the wall thickness, d_{in} is the internal column diameter, λ_w is the wall conductivity, d_{ex} is the external column diameter, h_{ex} is the external convective heat coefficient, h_w is the internal heat transfer coefficient and d_{ln} is defined as follows:

$$d_{ln} = \frac{(d_{ex} - d_{in})}{\ln(d_{ex}/d_{in})} \tag{3.62}$$

The internal convective heat transfer coefficient between the gas and the wall column can be estimated with this correlation:

$$\frac{h_w d_{in}}{k_g} = 140 + 0.013396 \frac{d_{in}^2}{d_p k_g} Re \tag{3.63}$$

3.3.5 Fixed bed initial and boundary conditions

The final element necessary to execute the simulations are the initial and boundary conditions of the model. In the fixed bed experiments, the column is initially filled with an inert gas, helium, and does not contain any other component. Additionally, the column should be regenerated, which means that the adsorbed concentration is zero. The temperatures in the fluid phase, solid and wall are all equal to the temperature of the inlet. Mathematically, this can be expressed with the equations below:

Initial conditions

$y_i = q_i = 0 \; \forall \; z$, except for inert

$y_{inert} = 1$

$T_g = T_s = T_w = T_{inlet}$

Boundary conditions

Entering conditions, $z = 0$

$$u_{i,inlet} c_{inlet,i} = u_i c_i - \varepsilon_b D_{ax} C_T \frac{\partial y_i}{\partial z}$$

$$u_{i,inlet} C_{T,inlet} C_p T_{inlet} = u_i C_p T_g C_T - \lambda \frac{\partial T_g}{\partial z}$$

$$u_{i,inlet} C_{T,inlet} = u_i C_T$$

Exiting conditions, $z = L$

$$\frac{\partial c_i}{\partial z} = 0$$

$$\frac{\partial T_g}{\partial z} = 0$$

$$P = P_{out}$$

where P_{out} is the pressure at the exit of the column.

4 Experimental setup

The fixed bed experiments were conducted in the PSA unit shown in Figure 4.1. A simplified scheme of the experimental setup is presented in Figure 4.2. This unit is generically composed of 4 columns and a set of different valves that allow the unit to run different regeneration cycles. Since the equipment was used to run breakthrough curve experiments, only one column was necessary. The unit was designed to run in a pressure interval of 0.1 – 70 bar and 298 – 550 K. The unit allows the connection of diverse analytical methods for analysis of the outlet components and includes an injection of a tracer gas (argon) to determine the existence of flow variations. For the CO_2/CH_4 separation, mass spectroscopy (MS) was the method used to identify the composition of the outlet stream.

Figure 4.1 – Experimental PSA unit used for the fixed bed experiments

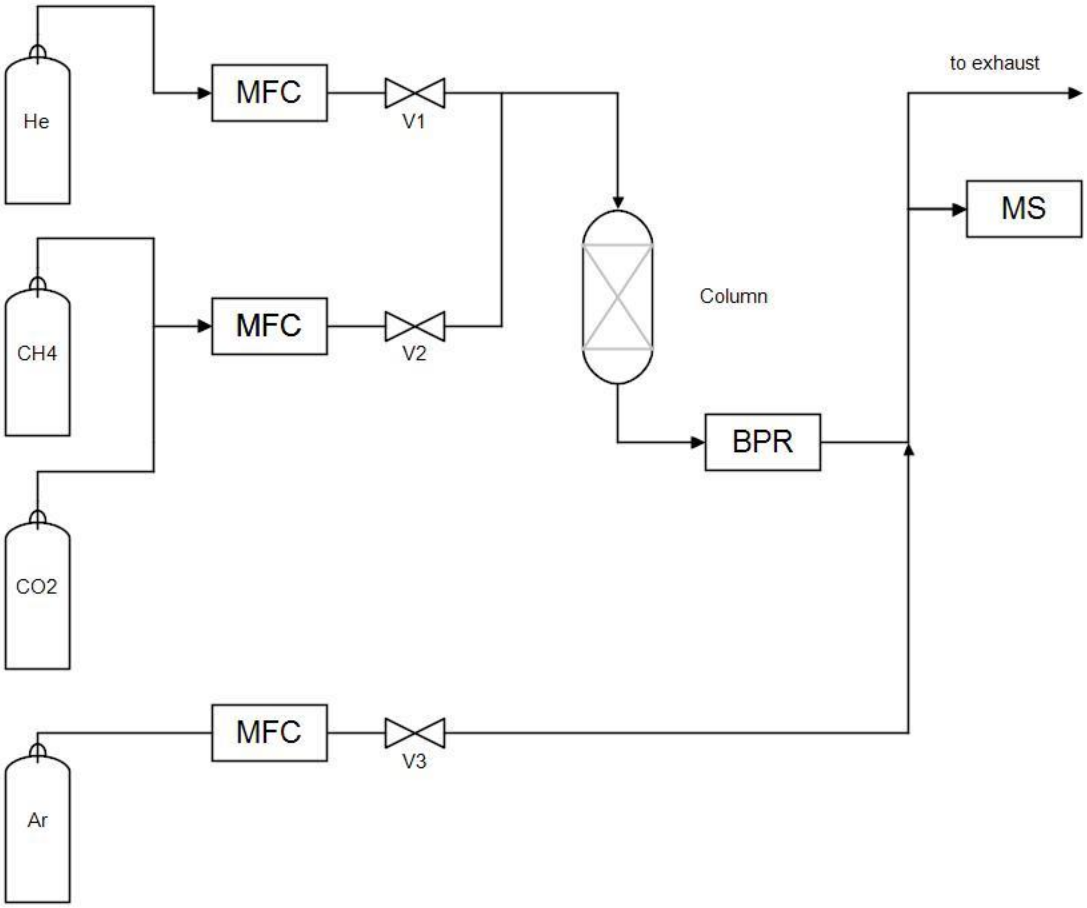

Figure 4.2 – Simplified diagram of the experimental setup used for the breakthrough curve experiments. Abbreviations are as follows: MFC: mass flow controller, BPR: back-pressure regulator, MS: mass spectrometer.

The column is made of a steel tube 2.54 cm external diameter and 0.56 m long. The temperature changes inside the column were monitored by four thermocouples located at 0.05 m, 0.20 m, 0.35 m and 0.5 m from the feed inlet. These are located in the centre of the column. The device used for that purpose might affect the measurement of the last thermocouple, reducing the value.

The columns are located inside a ventilated oven. However, the ventilated air does not contact directly with the column. This means that while this is technically a case of forced convection, the overall heat transfer coefficient should not assume high values. In other words, it is rather a transition regime between forced and natural convection.

Table 4.1 summarizes the characteristics of the column, adsorbent and fixed bed experiments.

Table 4.1 – Characteristics common to all fixed bed experiments

Packed column	
Length (m)	0.56
External diameter (m)	0.0254
Internal diameter (m)	0.0211
Bed voidage	0.377
Bed density ($kg \cdot m^{-3}$)	660
Particle adsorbent	
Shape	Cylindrical
Mass (kg)	0.11789
Diameter (m)	9.0×10^{-4}
Length (m)	1.8×10^{-3}
Particle density ($kg \cdot m^{-3}$)	1060
Feed	
Temperature (K)	313.15
Composition	90 % CH_4, 10 % CO_2
Pressure (bar)	From 5 to 70

The breakthrough curves were measured at different inlet pressures, ranging from 5 to 70 bar. The experiment at 70 bar was carried out with two different feed flow rates. The differing features between the experiments are presented in Table 2.

Table 4.2 – Feed pressure and flow rates for the breakthrough curve experiments.

Run	1	2	3	4	5	6	7	8	9	10
Pressure (bar)	5	10	15	20	30	40	50	60	70	70
Feed flow rate (SLPM)	0.5	0.5	0.5	0.5	0.5	0.5	0.5	0.5	0.5	1.0

5 Results and Discussion

5.1 Adsorption equilibrium

The adsorption equilibrium of CH_4 was measured at 298 and 343 K in the pressure range of 0 to 65 bar. The isotherms are presented in Figure 5.1. The adsorption equilibrium of CO_2 was examined at the same temperatures and in the pressure range of 0 to 30 bar, with the results being presented in Figure 5.2. The measurements were made in a Belsorp Max Instrument.

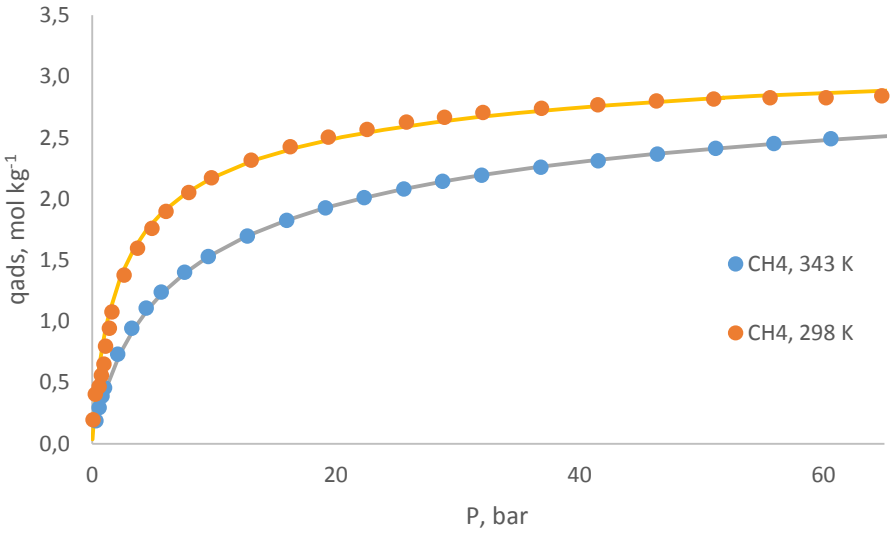

Figure 5.1 - Adsorption isotherms of CH_4. The points are the experimental data, the lines represent the multisite Langmuir fit.

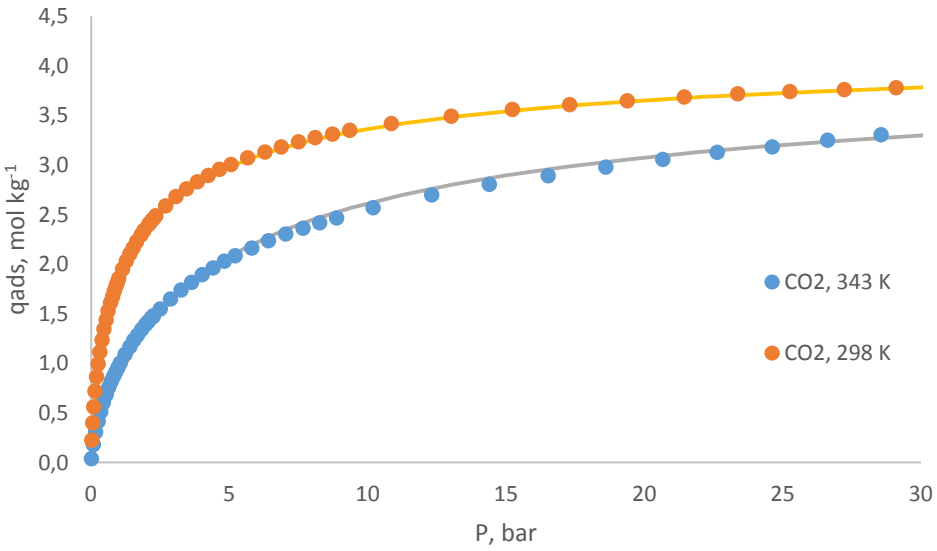

Figure 5.2 – Adsorption isotherms of CO_2. The points are the experimental data, the lines represent the multisite Langmuir fit.

The feed stream in the breakthrough curve experiments will consist of 10 % CO_2 and 90 % CH_4. The partial pressure of carbon dioxide will thus only go as high as 7 bar (for the 70 bar experiment) while the methane partial pressure will reach 63 bar. The adsorption equilibrium of the two components was therefore studied in different pressure ranges.

In both cases, the experimental data was fitted with the multisite Langmuir isotherm. The CH_4 data was fitted by minimizing the sum of the relative errors, while the CO_2 parameters were obtained by minimizing the sum of the relative and absolute errors. As explained in the section dedicated to the multisite Langmuir model, the product of the number of neighbouring sites occupied by a particle by the number of adsorption sites must remain constant for all thermodynamic consistency. To facilitate the optimization of the parameters, the CO_2 data was fitted first since it is usually harder to fit given the steepness of the isotherm. The CH_4 isotherm was then fitted with an added restriction so that the thermodynamic requirement was satisfied. The parameters were optimized with a code written in Python and are presented in Table 1.

Table 5.1 – Fitting parameters of the multisite Langmuir model.

	q_m / mol·kg^{-1}	k_0 / Pa^{-1}	-ΔH / J·mol^{-1}	a	$q_m \cdot a$
CH_4	3.493	8.169×10^{-10}	21 410	2.047	7.151
CO_2	4.299	8.436×10^{-10}	23 201	1.663	7.151

The Python program uses the Nelder-Mead optimization method to determine the fitting parameters for different isotherms. The user can choose which isotherm model to use and which type of error to minimize. That information and the experimental data are read from a properly formatted excel file. The initial guess is written directly in the code. The program outputs a plot with the experimental data and the fitting model, the fitting parameters and the details of the optimization.

The quality of the experimental data and of the fitting model can be accessed by plotting the respective Virial curves. These consist in plotting the natural logarithm of P/q_{ads} as a function of the amount adsorbed, q_{ads}. For low values of adsorbent loading, the obtained graph should be linear, with the slope corresponding to the Henry constant of the component. This plot allows the removal outliers, which clearly stand out of the linear region of the graph. The Virial curves of the experimental data and of the fitting of the multisite Langmuir model are presented in Figures 5.3 and 5.4.

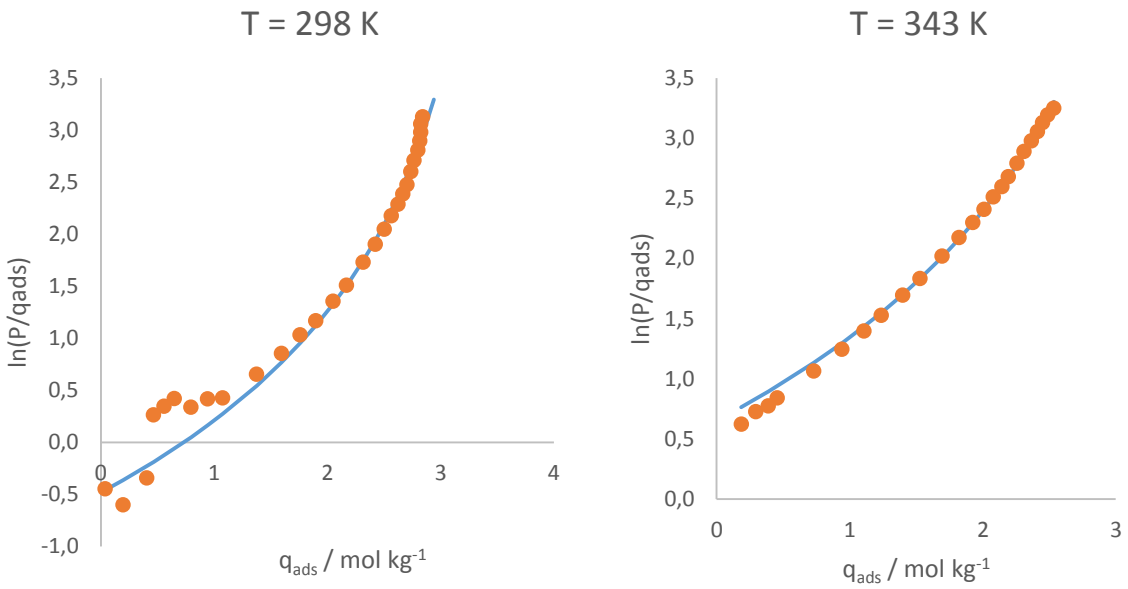

Figure 5.3 – Virial plots for methane. Points are the experimental data and the solid lines represent the multisite Langmuir fit.

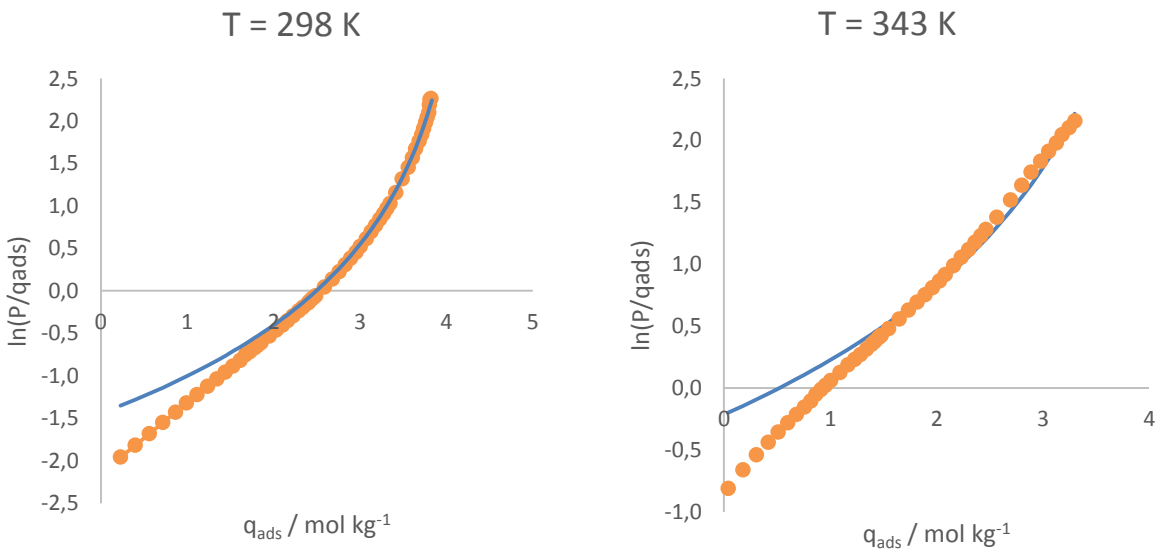

Figure 5.4 – Virial plots for carbon dioxide. Points are the experimental data and the solid lines represent the multisite Langmuir fit.

From the analysis of the Virial plots it can be concluded that all cases are linear for low values of q_{ads}, except for the isotherm of methane at 298 K. However, the respective mathematical model does not appear to have been affected by this. A difference between the data and the model can be seen in the CO_2 isotherms for low adsorbent loading. This is probably due to the fact the carbon dioxide isotherm is quite steep in that region, making the

mathematical fitting more difficult. Overall, it can be concluded that a satisfactory fit was reached.

From the comparison of the experimental data with fitted curves, it can be concluded that an overall good fit was reached. Furthermore, the obtained parameters are within the expected values: the heats of adsorption for the two components are similar to those found elsewhere [23], [24], [25] and the value of the a parameter is not too high (a value above 20 is rather unrealistic, and would suggest that the model is not appropriate)[15]. In fact, this parameter is directly related to the size of the particles, and should be in accordance with that property.

From the analysis of the isotherms, it is clear that the adsorbent as a greater affinity towards CO_2, given its higher saturation capacity and the greater steepness of the curve when compared with the methane isotherm.

With the values of the isotherm parameters, it is possible to predict the shape of the multicomponent isotherms with the multicomponent extension presented in equation (3.6). Figures 3 and 4 present these curves at 313 K, for a system with 90 % methane and 10 % carbon dioxide, the same as the feed used in the fixed bed experiments.

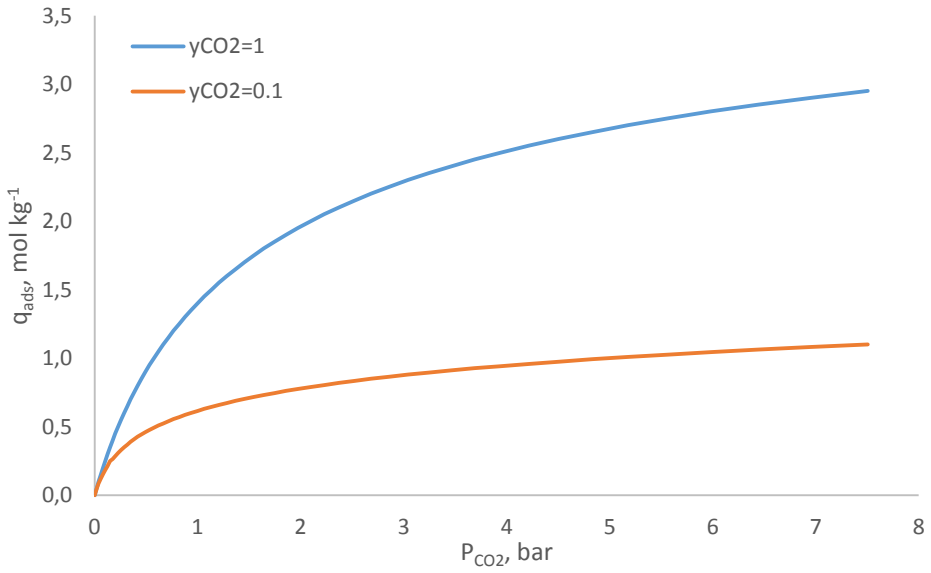

Figure 5.5 – Carbon dioxide isotherms at 313 K: pure component and in a mixture with 90 % methane and 10 % carbon dioxide.

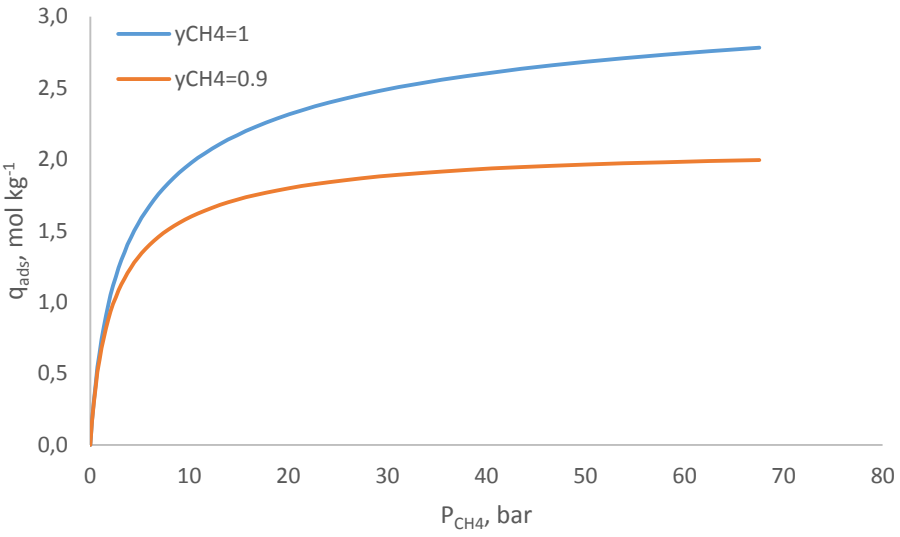

Figure 5.6 – Methane isotherms at 313 K: pure component and in a mixture with 90 % methane and 10 % carbon dioxide.

These curves are relevant when analysing the capacity exhibited by the adsorbent in the fixed bed experiments. It can also be concluded that the selectivity exhibited by the adsorbent is quite poor. That does not mean that it is not an effective adsorbent for this separation. If a component diffuses more rapidly through the pores, it will be preferentially adsorbed in the early stages of the process, regardless of the equilibrium state [26]. In other words, it is possible to achieve the separation if the kinetic selectivity is important.

5.2 Adsorption kinetics

The adsorption kinetics experiments were performed at low pressures, so it can be assumed that they operated in the linear zone of the isotherms. In addition, they can be considered isothermal. These conditions allow the use of the mathematical described in Chapter 3 to fit the experimental data.

The uptake curves were measured in a volumetric unit. Data was received every second for the first isotherm point. Equilibrium was assumed if the pressure variations were inferior to $1 \times 10^{-3}\ kPa$ for a period of 9999 seconds, the maximum allowed by the equipment.

The results of the experiments described for the kinetics of CO_2 and CH_4 are presented in Figure 5 and 6. In Figure 5, the curves are presented as a function of time, and clearly show that carbon dioxide diffuses through the micropores at a much faster rate than methane. Equilibrium is reached with CO_2 after approximately 800 seconds (around 13 minutes), at a time when the q/q_{eq} factor for CH_4 is only at 0.07. Equilibrium for methane is reached after over 90 000 seconds, which corresponds to 25 hours.

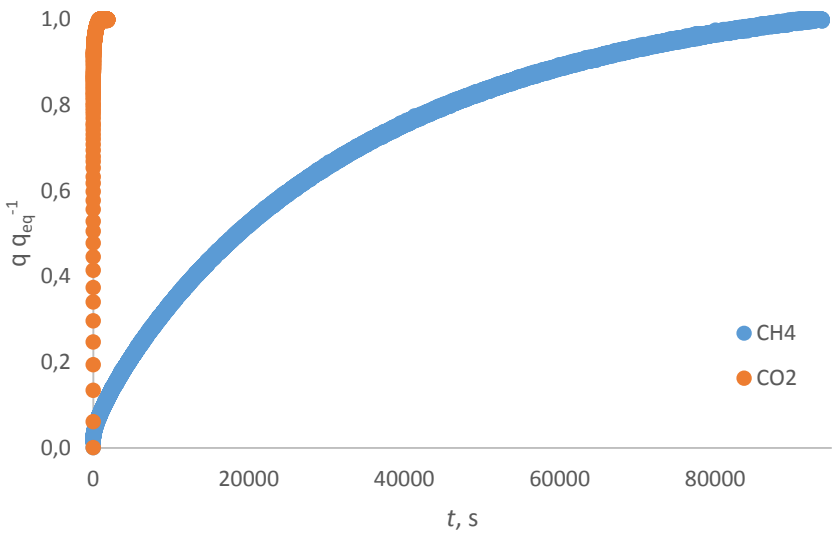

Figure 5.7 – Adsorption kinetics of CO_2 and CH_4 at 298 K.

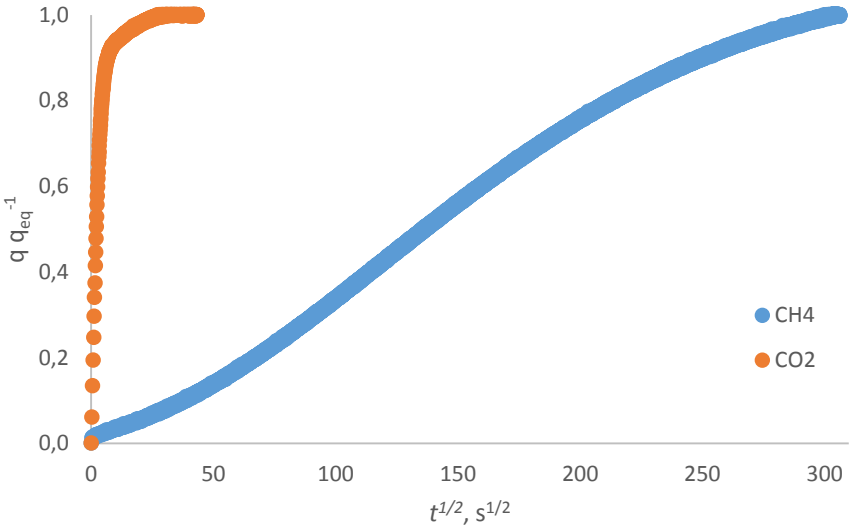

Figure 5.8 - Adsorption kinetics of CO_2 and CH_4 at 298 K against the square root of time.

The effect of the surface barrier at the mouth of the micropore is visualized by a small slope in the initial moments [25]. To enhance this effect, the same results were plotted over the square root of time, as presented in Figure 6. The slope is clearly visible in the methane curve, indicating that the constriction at the mouth of the micropore has an important contribution to the overall diffusion resistance. For carbon dioxide, however, this effect is not observed. This difference in the kinetic behaviour of the two components is expected, given that CO_2 is the smaller molecule of the two, with a kinetic diameter of 3.3 Å against 3.8 Å of methane.

The parameters that affect the kinetics of methane were estimated using gPROMS with the model described in Chapter 3.2. Two different sets of parameters were considered, with the results being presented in Figure 5.9.

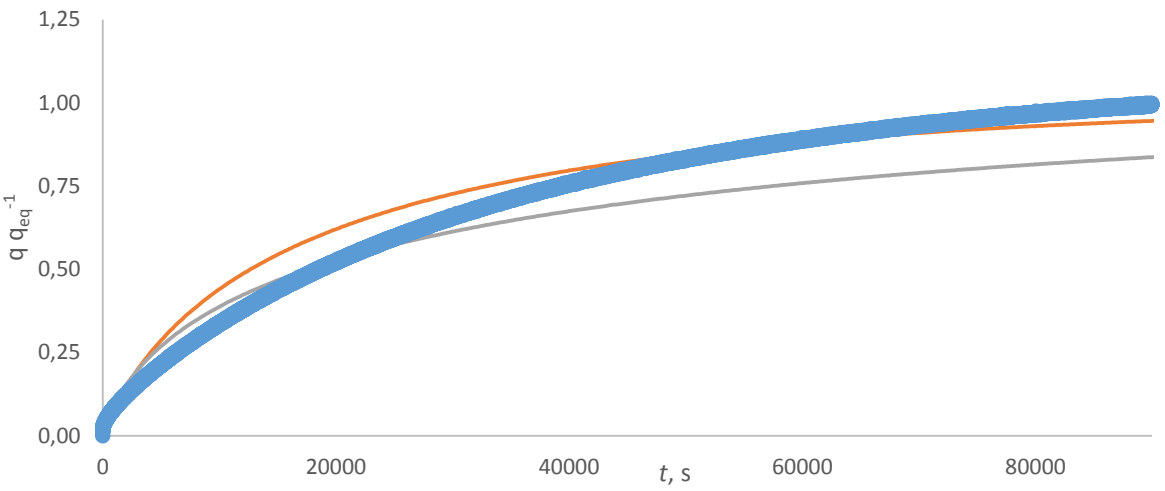

Figure 5.9 - Adsorption kinetics of CH_4 at 298 K with the solid lines representing the mathematical models.

The orange curve corresponds to $\frac{D_c}{r_c^2} = 3.0 \times 10^{-6}\ m^2\ s^{-1}$ and $k_b = 6.5\ \times 10^{-5} s^{-1}$. The grey curve corresponds to $\frac{D_c}{r_c^2} = 1.2 \times 10^{-6}\ m^2\ s^{-1}$ and $k_b = 1.0\ \times 10^{-4} s^{-1}$. The difference between the experimental data and the model may be due to the resistance not being completely controlled by the constriction at the pore mouth.

The same procedure was followed for CO_2. The constriction at the pore mouth does not play a part in the carbon dioxide diffusion, so $k_b = 0$. The grey line corresponds to $\frac{D_c}{r_c^2} = 1.0 \times 10^{-3}\ m^2\ s^{-1}$ and the yellow line $\frac{D_c}{r_c^2} = 7.48 \times 10^{-4}\ m^2\ s^{-1}$.

Since the barrier mass transfer resistance term is only negligible for carbon dioxide, the kinetics of this component can be fitted with the simplified model presented in Chapter 3.2. The data was fitted by minimizing the square of residuals, in a program written in Python. The value obtained for the diffusion constant was: $K_{\mu,CO_2} = 1.695\ \times 10^{-4}\ s^{-1}$ (represented by the orange line). Considering equation (3.22), these values are in accordance with each other.

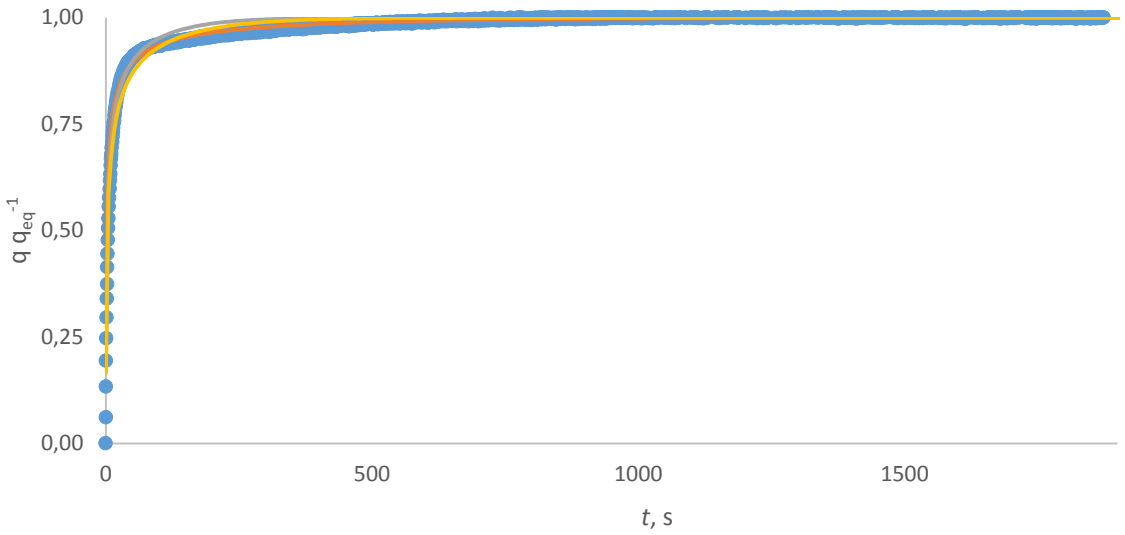

Figure 5.10 – Adsorption kinetics of CO_2 at 298 K with the solid lines representing the mathematical models.

The Python program developed for adsorption kinetics uses the Nelder-Mead optimization method to fit the experimental data of uptake curves and obtain the diffusion constant of the respective component. Before proceeding to the fitting of the experimental data, the roots of equation (3.24) are determined with Python's *fsolve* function. In the same manner as for the isotherm program, data are read from an excel file while the initial guess for the roots and for the diffusion constant are written in the code. The program outputs a plot with the data and the fitting model, the value of the diffusion constant and the details of the optimization. In addition, the program also outputs the list of the roots of equation (3.24), for the user to check if they are valid. The roots of that equation are periodic, but solvers sometimes require a very precise initial guess to find all of them.

5.3 Fixed bed experiments

The first step in the analysis of the breakthrough curve results is the treatment of the MS data. The MS analysis is not made immediately after the column outlet, but instead after going through the back pressure regulator and being mixed with a constant stream of argon. In addition, the data is delivered in the form of intensity signals, which do not correspond directly to the molar fraction. In order to obtain the proper breakthrough curves, first it is necessary to "normalize" the signals, by multiplying them by an appropriate number so that the equilibrium value is the expected one. Afterwards, the concentration histories at the exit of the column are obtained by solving a mass balance involving the added argon stream.

The analysis of the breakthrough curves was made by treating the mass spectroscopy (MS) signal and also by using a tracer gas in the system (Argon) to detect flow variations. The initial step is to make a mass balance at the junction of the argon stream with the mixture exiting the column and determine the total flow exiting the column (that changes with time). The other components are then determined from component mass balances.

The experimental breakthrough curves as well as the respective temperature histories are presented below. The points represent the experimental data, the lines the simulated curves.

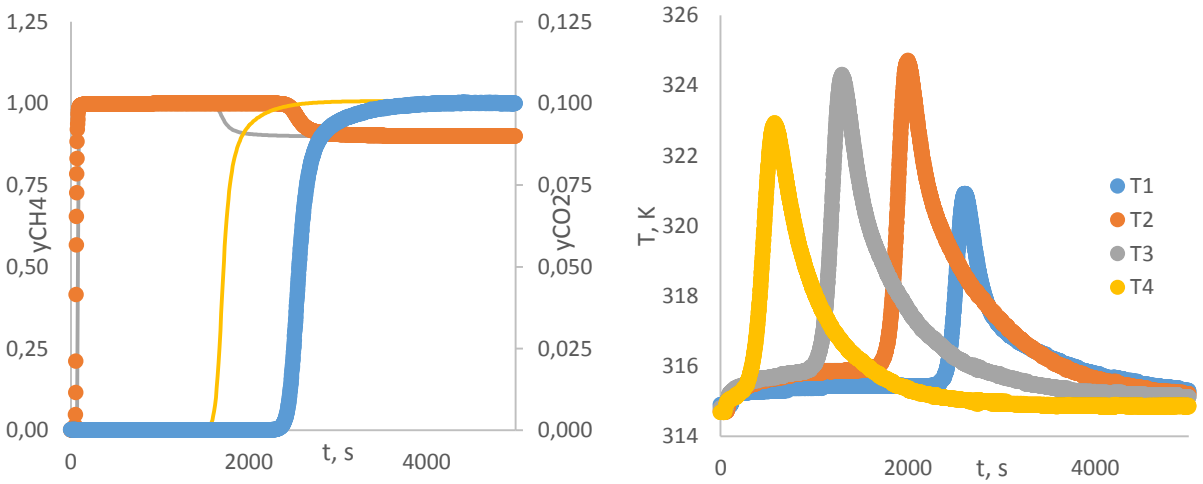

Figure 5.11 – Breakthrough curves (left) and temperature histories (right) at 5 bar.

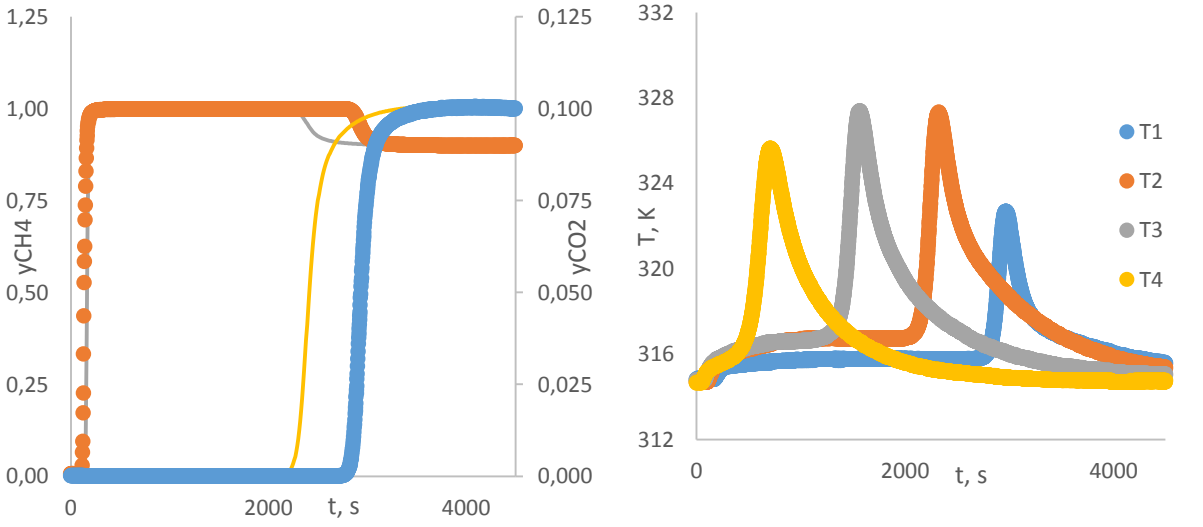

Figure 5.12 – Breakthrough curves (left) and temperature histories (right) at 10 bar.

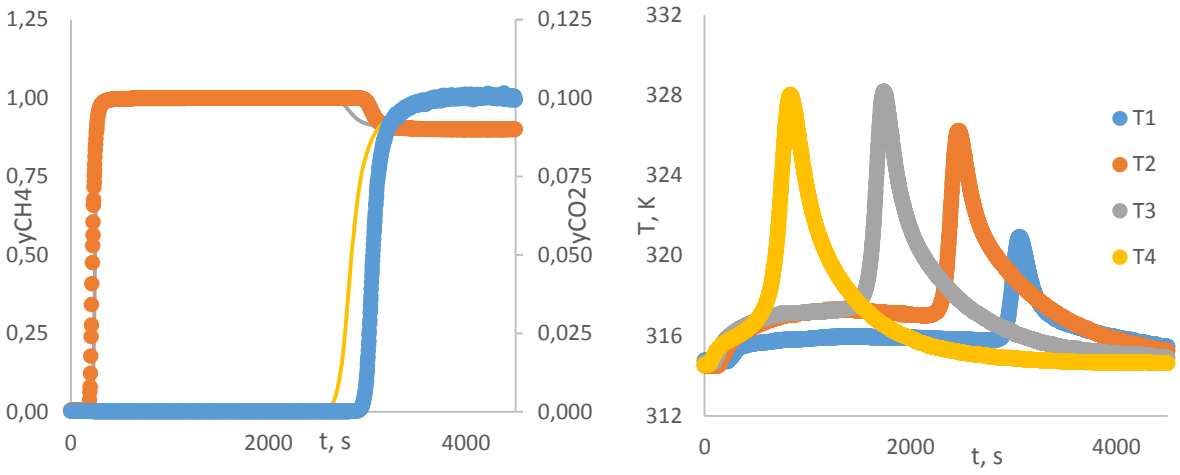

Figure 5.13 – Breakthrough curves (left) and temperature histories (right) at 15 bar.

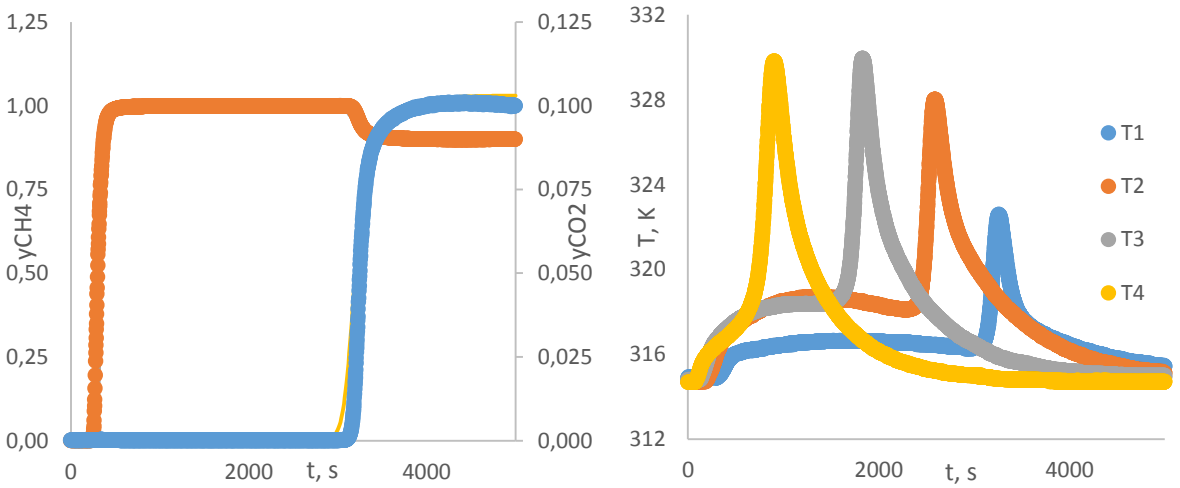

Figure 5.14 – Breakthrough curves (left) and temperature histories (right) at 20 bar.

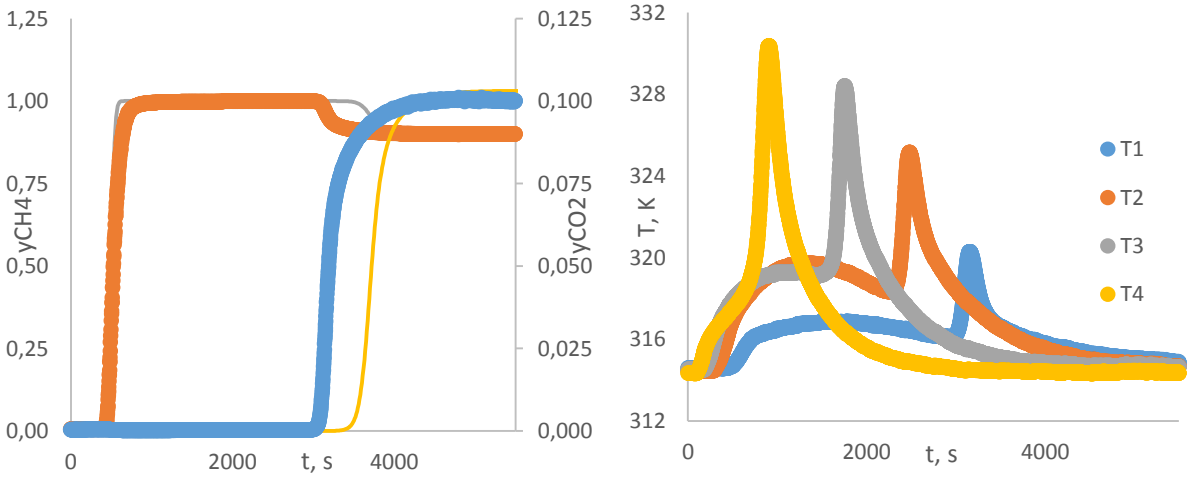

Figure 5.15 – Breakthrough curves (left) and temperature histories (right) at 30 bar.

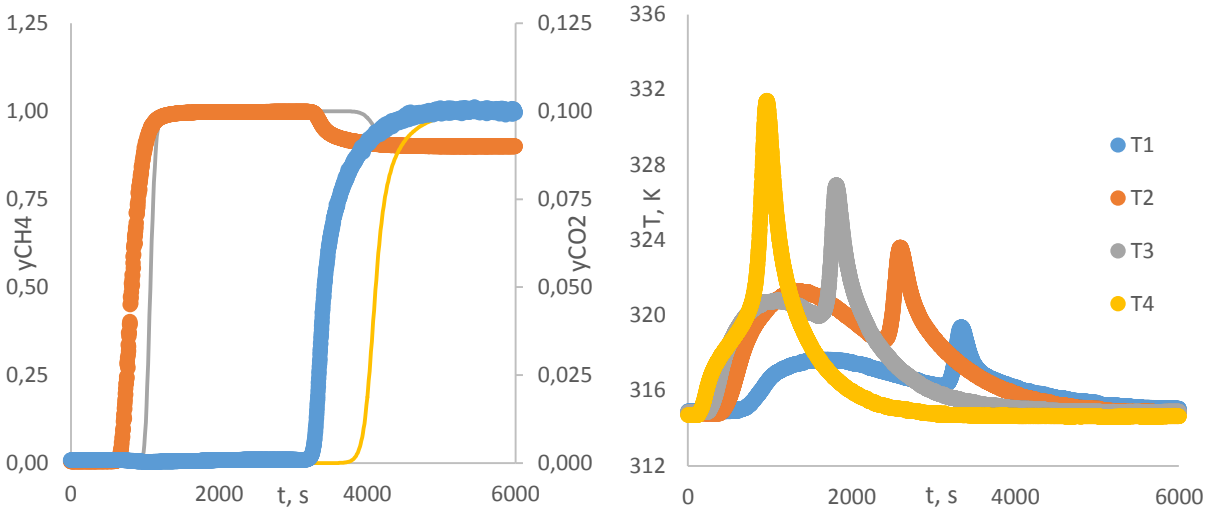

Figure 5.16 – Breakthrough curves (left) and temperature histories (right) at 40 bar.

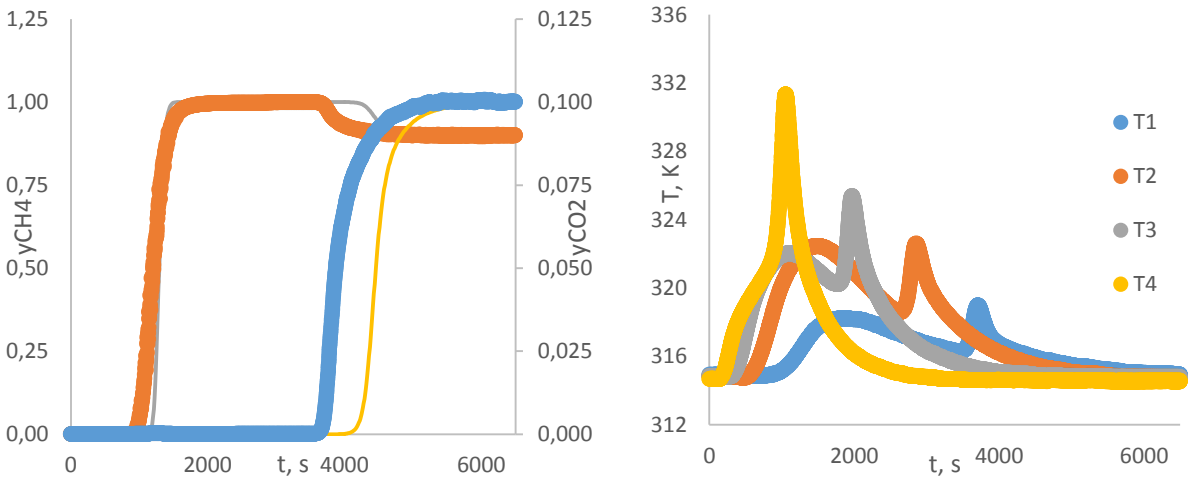

Figure 5.17 – Breakthrough curves (left) and temperature histories (right) at 50 bar.

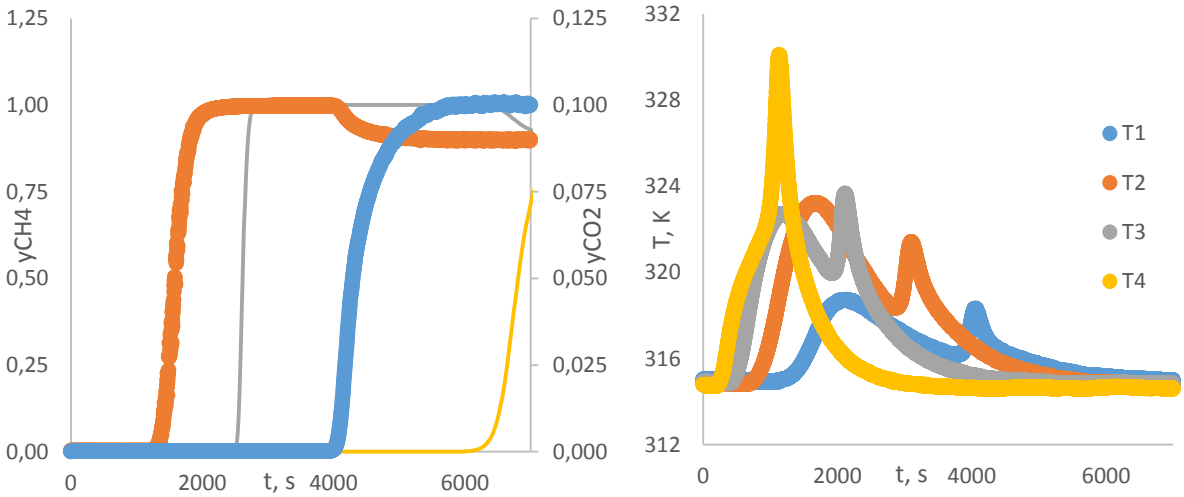

Figure 5.18 – Breakthrough curves (left) and temperature histories (right) at 60 bar.

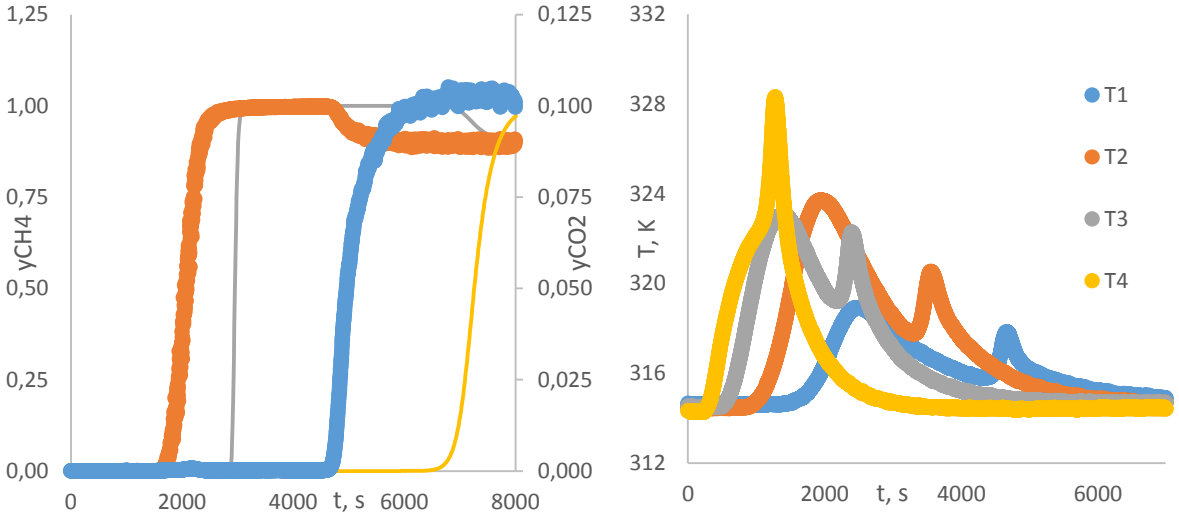

Figure 5.19 – Breakthrough curves (left) and temperature histories (right) of the first experiment at 70 bar (Q = 0.5 SLPM).

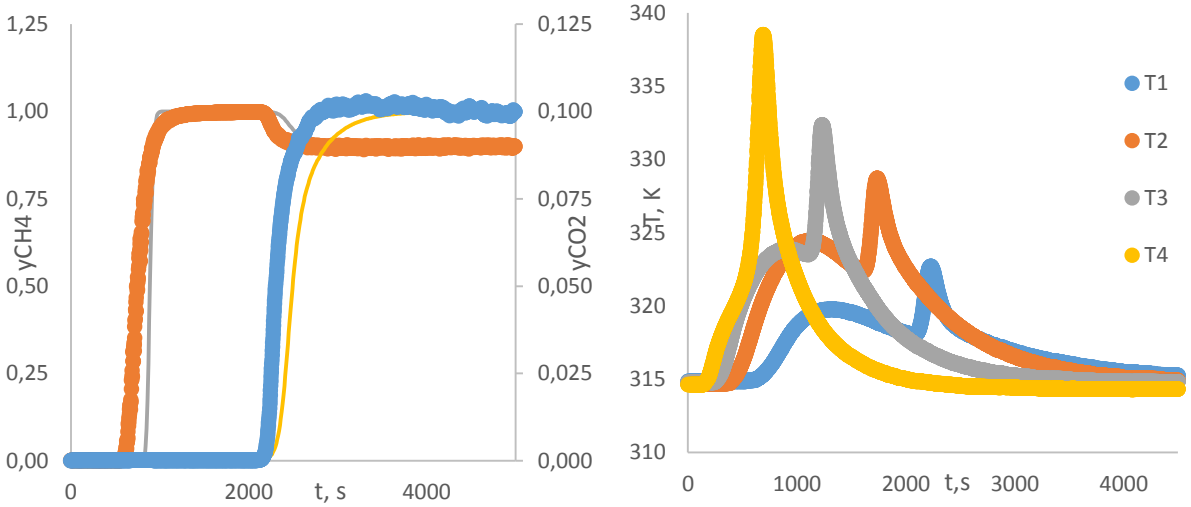

Figure 5.20 – Breakthrough curves (left) and temperature histories (right) of the second experiment at 70 bar (Q = 1.0 SLPM).

It is possible to calculate the capacity of the column from the breakthrough curves. For the CO_2, the amount adsorbed corresponds to the negative integral of the flux breakthrough curve. That value divided by the adsorbent mass present in the column will yield the column capacity for carbon dioxide. The obtained capacities were compared with the single and multicomponent isotherms originally presented in Figure 5.6.

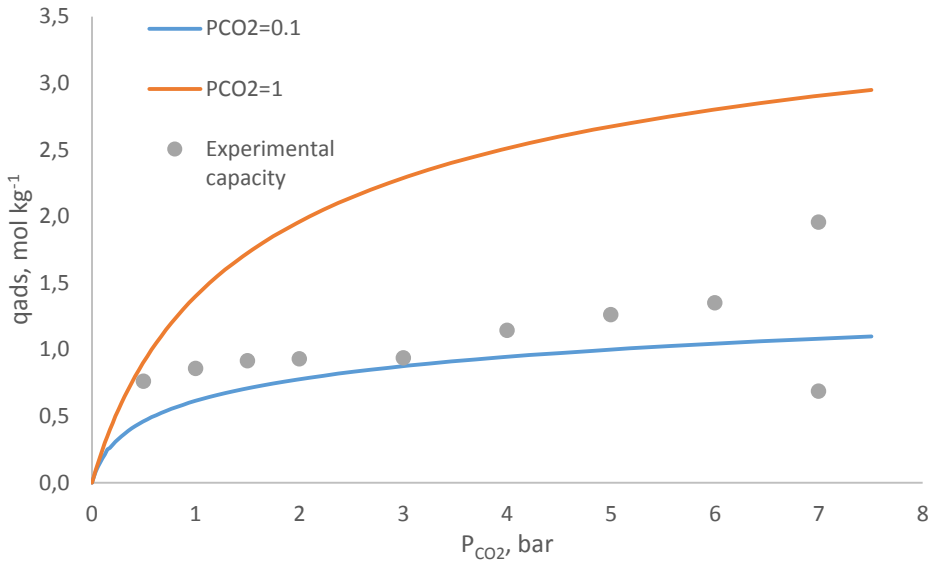

Figure 5.21 – Comparison between the single and multicomponent carbon dioxide isotherms and the experimental capacity determined by binary breakthrough curves.

From the analysis of Figure 5.20, it can be concluded that the CO_2 capacity is higher than the one predicted by the equilibrium between the two species (the blue line). That is in accordance with the fact that the adsorbent is kinetically controlled. However, given that carbon dioxide diffuses through the micropores at a much faster rate than methane, the experimental capacity was expected to be higher, closer to the values of the CO_2 single component isotherm (the orange line). Furthermore, the points representing the capacity of the column at 70 bar deviate considerably from the trend shown by the remaining experiments. In addition, those two experiments should exhibit the same adsorption capacity, yet the two values are very different, with the run with a 0.5 SLPM feed stream having the higher value.

These results strongly suggest that most of the experiments were made with a column that was not fully regenerated. In fact, the very first experiment was the one at 70 bar and a feed of 0.5 SLPM, and its column capacity stands out from the others. It is possible that the first run was the only one with an "empty column" and that the subsequent experiments were made with columns that had a certain amount of methane and carbon dioxide still adsorbed from the beginning. Most of the experiments were made in consecutive days.

It has been observed and described in activated carbon [27], [28] that some components adsorb irreversibly in the adsorbent, causing the isotherms to exhibit hysteresis and the adsorbent to have an "effective capacity" that is lower than expected. However, the adsorption and desorptiob isotherms were measured twice and were reproducible, as well as not having shown any hysteresis. This means that this phenomenon does not happen in this adsorbent.

Another possibility is that the kinetic behaviour of the components in the mixture is different from the one as single components in the mixture. As methane is nine times more

abundant in the feed than carbon dioxide but diffuses slower, it may obstruct the entrance of the micropores and difficult the passage of CO_2.

5.4 Simulations

The simulations were carried out in gPROMS. The chosen model considered diffusion in the macropores and micropores as well as resistance in the film. The Ergun equation was used for the momentum balance and the heterogeneous model applied for the energy balance. The discretization method used was centered finite differences, with 300 discretization intervals for the experiments until 40 bar and 400 intervals for the experiments at 50 bar and higher. The solution points were reported at 10 second intervals, and the gPROMS numerical solver used was SRADAU. The simulated curves were already present in the previous section, but are presented again for a more detailed analysis.

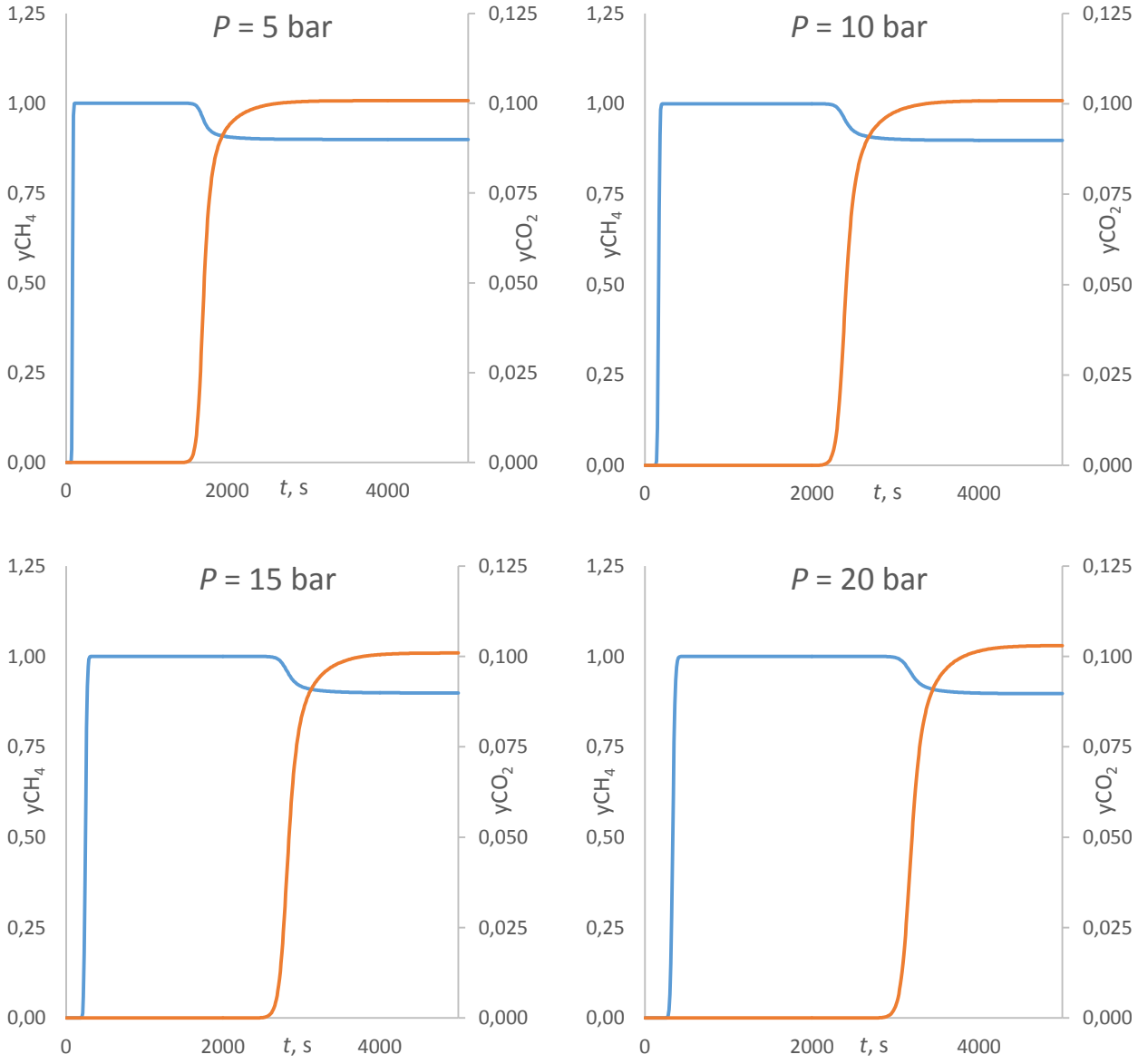

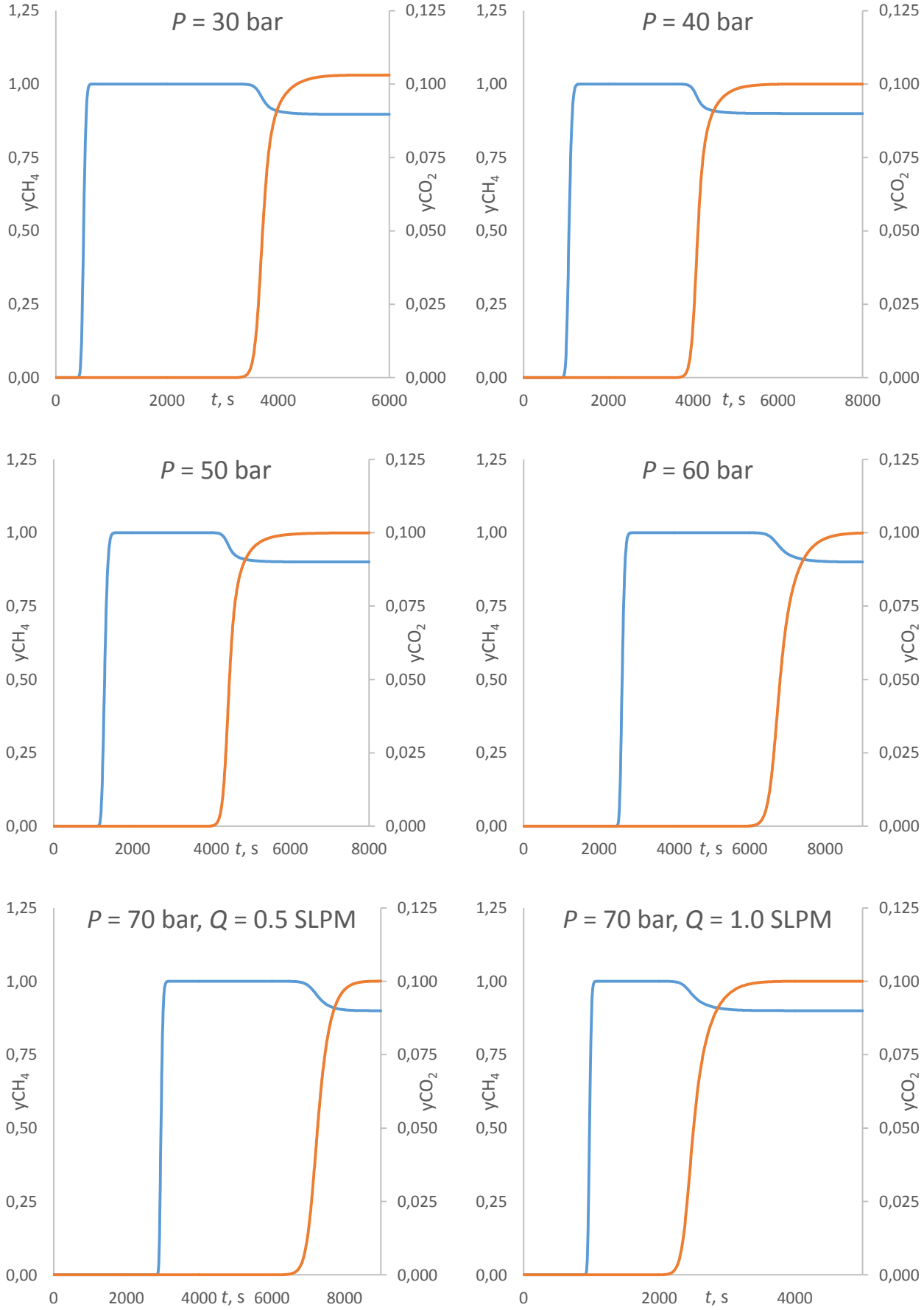

Figure 5.22 – Simulated breakthrough curves.

From the analysis of the curves presented in Figure 5.21, it appears that the gPROMS program was effective at simulating the mathematical model. The methane roll-up is present from being displaced by CO_2, the mostly adsorbed compound and the breakthrough times happen later as the pressure increases. Nonetheless, the simulated curves do not correspond to the experimental ones. It should be noted that while the higher pressure simulations exhibit higher breakthrough times than the experimental curves (which is consistent with the possibility of having used a non-regenerated column), the low pressure simulations (at 5 and 10 bar) actually have earlier breakthrough times than the respective experiments. Assuming that the simulations were accurately calculated, this fact suggests that the model itself may not be sufficiently detailed to describe a kinetically controlled system such as the one studied in this work.

The temperature histories in different sections of the column were also simulated, and are presented in Figure 5.23.

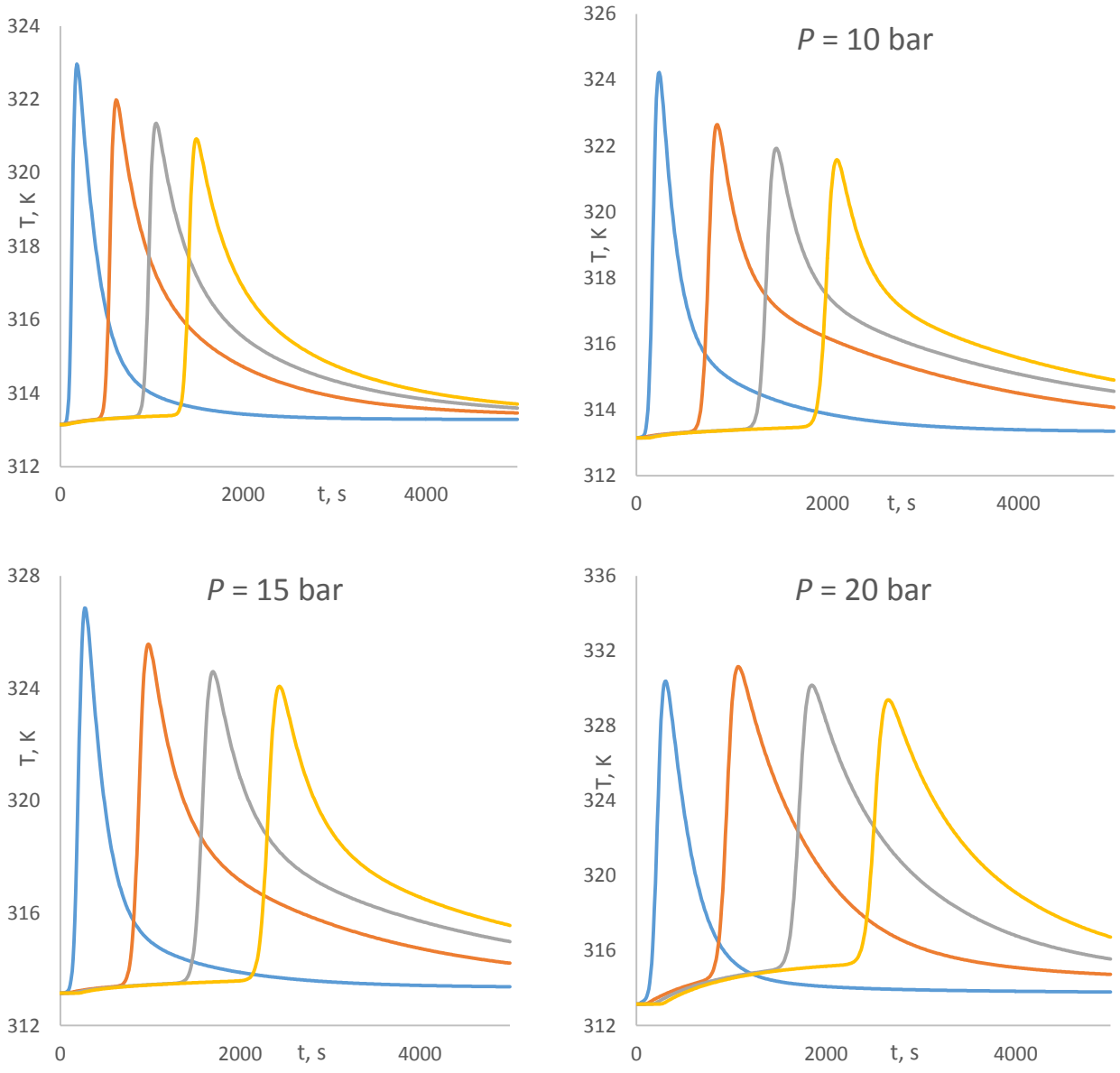

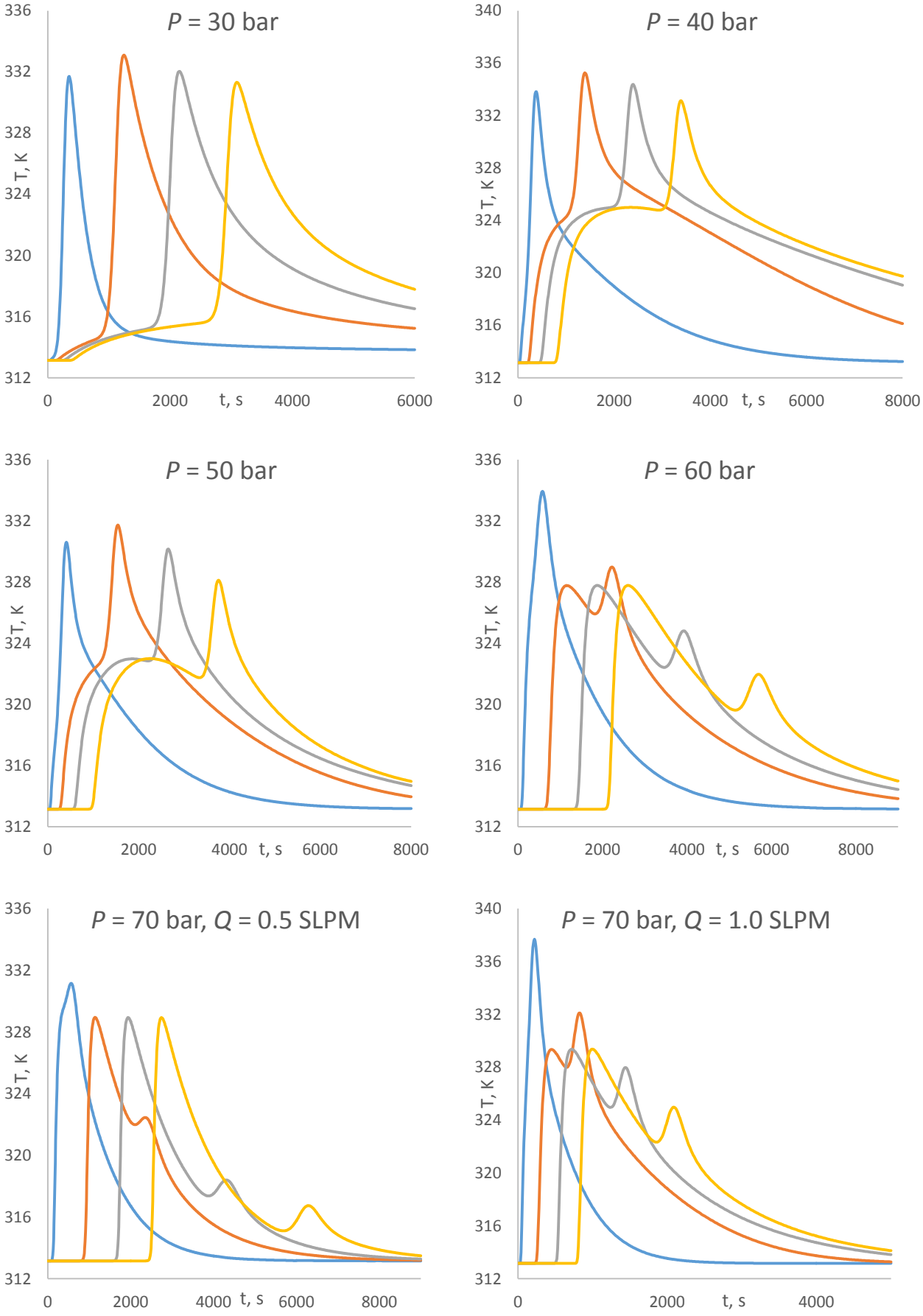

Figure 5.23 – Simulated temperature histories.

The values of the overall heat transfer coefficient and of the film heat transfer coefficient between gas and the wall were estimated by comparison between the simulated and experimental curves. The overall heat transfer coefficient controls how quickly the temperature returns to the initial value after the peak. A higher value causes a faster cooling. The film heat transfer between the gas and the wall is related to the height of the peak, in other words, the highest temperature reached. A lower value of this parameter implies a higher peak. These parameters were thus iterated until a satisfactory fit was reached.

The simulation of the breakthrough curves was also attempted with Python. The version used was Python 3, which has several solvers for ordinary differential equations but does not yet have one for partial differential equations. Therefore, the numerical method used was the method of lines, where the equations are discretized in space using centered finite differences. A system of ordinary differential equations in time is obtained that was then solved by Python's *odeint* solver, based on LSODA.

The approach to writing the code consisted in simulating models with increasing levels of complexity. A code for the simulation of a single component breakthrough curve in a system with macropore, micropore and film mass transfer resistances was successfully achieved. The values of the parameters are all written in the code. The code outputs a graph with the simulated breakthrough curve. Figure 5.23 presents a single component breakthrough curve simulated for a generic case with $Pe = 100$.

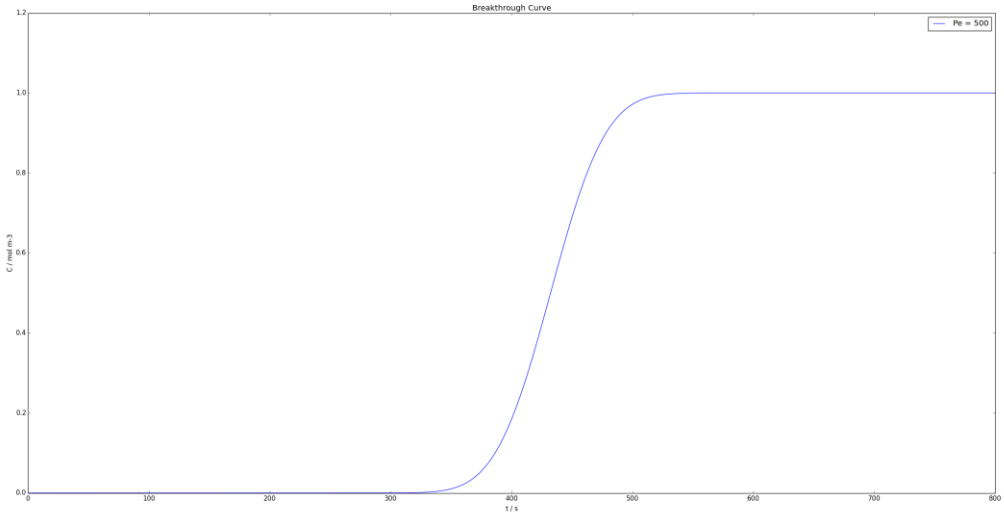

Figure 5.24 – Single component breakthrough curve obtained with the method of lines method.

6 Conclusions

In this work, the KP – 407 adsorbent was studied for the separation of carbon dioxide from methane. The adsorption equilibrium isotherms were measured at 298 K and 343 K and the experimental data was fitted with the multisite Langmuir model. Although presenting low equilibrium selectivity, the adsorbent presents a great kinetic selectivity where CO_2 is the fastest species, therefore, this adsorbent is adequate for the separation. Additionally, the uptake curves analysed allowed concluding that the pore mouth has a significant contribution to the overall micropore mass transport resistance to CH_4.

Fixed bed experiments were performed to measure the breakthrough curves of a mixture of 90 % methane and 10 % carbon dioxide, at pressures ranging from 5 to 70 bar. As expected, CO_2 was the preferentially adsorbed component. The column capacities for carbon dioxide were calculated from the breakthrough curves and compared with the respective single and multicomponent isotherms. The calculated capacities did not present a general trend and they were significantly lower than expected, considering the huge difference in diffusivities between the two components. This may be due to an incomplete regeneration of the column prior to the execution of each breakthrough curve measurement. The cause of this may be related to the regeneration step having lasted for a shorter time than necessary or due to an undetected hysteresis in the isotherms, causing a certain amount of the components to remain irreversibly adsorbed. Additionally, the adsorption kinetics might also have a more complex behaviour than originally considered. The diffusivities of the two components may be different in a mixture than as pure components and may also be affected by pressure.

Different models were studied to describe the equilibrium, kinetics and breakthrough curves obtained experimentally. Some of the most common adsorption isotherms were considered for the mathematical fitting to the experimental data. The multisite Langmuir model was chosen given its ability to fit the experimental values and simple multicomponent extension. This last characteristic is important given the fact that a multicomponent isotherm was employed when simulating the breakthrough curves, and a more complex model may unnecessarily increase the computational time. A model to calculate the diffusivity of a species in a system where both the micopore and pore mouth resistances are important was presented, together with a simplification for the cases where the pore mouth could be neglected. A mathematical model to simulate the breakthrough experiments was described. Several different alternatives were considered, depending on the limiting mass transport resistances. The proposed model includes the mass, momentum and energy balances. The simulated breakthrough curves did not fit to the experimental curves; the experiments may have been affected by an incomplete regeneration as explained.

A large part of the work was also dedicated to the development of Python programs. The programs are capable of finding the fitting parameters of different models of equilibrium and kinetics experimental data and simulate single component breakthrough curves. The simplicity of the programming language and the many numerical modules that can be used make Python a very effective tool for this type of work. However, the complexity of the complete fixed bed model and the limitations of the solvers available did not allow for a complete program to simulate breakthrough curves to be created during the period of this work.

Overall, the KP – 407 adsorbent studied in this work is a remarkable material for methane/carbon dioxide separation. Moreover, the experiments at 70 bar present novel data for the study of high pressure natural gas processing. Nevertheless, further work is necessary to fully understand and model the breakthrough curves and further on the whole PSA unit.

6.1 Future work and final assessment

This work found some limitations and challenges in both the experimental and modelling sections. While it was not possible to overcome all of them due to the time restrictions of the project, several approaches to future work are suggested.

The possibility that the fixed bed experiments were performed with a column that was not fully regenerated while require repeating these experiments. In addition to implementing longer regeneration cycles before each run, it may also be relevant to study in more detail the adsorption and desorption isotherms of the components, in order to identify any hysteresis related to irreversible adsorption. Given the importance played by kinetics in this adsorbent, it would also be pertinent to study the diffusivities of the two components further. For instance, analysing the uptake curves at different pressures and for components in a mixture. The analysis of this separation in PSA cycles is also a matter of interest.

The development and successful simulation of a more complex mathematical model is also a possibility. Part of this work also involved creating a software to describe adsorption phenomena. While programs to fit models to experimental data of equilibrium and kinetics experiments were successfully written in Python, the breakthrough curve program only considers a single component. Further work can be made to develop a more complete code in a free software. The existing programs can be further improved by implementing a more user-friendly interface.

At a personal level, this project allowed the understanding of the minutiae involved in modelling and the challenges faced in treating and interpreting experimental data. Moreover, it permitted the familiarization with new programming languages, Python and gPROMS. While the obtained results do not allow a definitive description of the adsorbent, this work presents what steps to take next in its study. In conclusion, the overall balance of the work is highly positive.

References

[1] Shimekit, B., Mukhtar, H., Natural Gas Purification Technologies – Major Advances for CO2 Separation and Future Directions, *Intech*

[2] Peters, L., Hussain, A., Follmann, M., Melin, T., Hägg, M.-B., CO_2 removal from natural gas by employing amine absorption and membrane technology - A technical and economical analysis, *Chemical Engineering Journal*, 172, 952-960, 2011.

[3] Mehra, Y. R., Gaskin, T. K., Guidelines offered for choosing cryogenics or absorption for gas processing, *Oil & Gas Journal*, 1999.

[4] Zhang, Y., Sunarso, J., Liu, S. and Wang, R., Current status and development of membranes for CO_2/CH_4 separation, *International Journal of Greenhouse Control*, 12, 84-107, 2013.

[5] Esteves, I. A. A. C., Lopes, M. S. S., Nunes, P. M. C., Mota, J. P. B., Adsorption of natural gas and biogas components on activated carbon, *Separation and Purification Technology*, 62, 281-296, 2008.

[6] Grande, C. A., Advances in Pressure Swing Adsorption for Gas Separation, *ISRN Chemical Engineering*, 2012

[7] Knaebel K. S., Adsorbent Selection, Adsorption Research, Inc., Dublin, Ohio 43016.

[8] Berstad, D., Nekså, P., Anantharaman, R., Low-temperature CO_2 removal from natural gas, *Energy Procedia*, 26, 41-48, 2012.

[9] Mieville, R. L. and Robinson K. K., Carbon Molecular Sieves and other porous carbons, Mega-Carbon Company.

[10] Skarstrom, C. W., Method and apparatus for fractionating gaseous mixtures by adsorption. U.S. Patent 2, 944, 627, 1960.

[11] Xu, J., Weist Jr., E. L., Six bed pressure swing adsorption process with four steps of pressure equalization, US Patent 6, 454, 838, 2002.

[12] Ruthven, D. M., Principles of Adsorption and Adsorption Processes, John Wiley & Sons, New York, NY, USA, 1984.

[13] Langmuir, I., The adsorption of gases on plane surfaces of glass, mica and platinum, *The Journal of the American Chemical Society*, 40, 1361-1403, 1918.

[14] Do, D. D., Adsorption Analysis: Equilibria and Kinetics. Imperial College Press, Department of Chemical Engineering, University of Queensland, Australia, 1998.

[15] Nitta, T., Shigetomi, T., Kurooka, M. and Katayama, T., An Adsorption Isotherm of Multi-Site Occupancy Model for Homogeneous Surface, *J. Chem. Eng. Japan*, 17, 1984.

[16] Cavenati, S., Separação de misturas $CH_4/CO_2/N_2$ por Processos Adsorptivos, PhD Thesis, Faculdade de Engenharia da Universidade do Porto, Porto, Portugal, 2005.

[17] Sircar, S., Influence of Adsorbate Size and Adsorbent Heterogeneity on IAST, *AIChE Journal*, 41, 1135-1145, 1995.

[18] Haynes, P. D., Lucas, S. K., Extension of a short-time solution of the diffusion equation with application to micropore diffusion in a finite system, *ANZIAM* J., 48, 503-521, 2007.

[19] Anand, K., Damodaran, S., Kinetics of Adsorption of Lysozyme and Bovine Serum Albumin at the Air-Water Interface from a Binary Mixture, *Journal of Colloid and Interface Science*, 176, 63-73, 1995.

[20] Da Silva, F. A., Cyclic Adsorption Processes: Application to Propane/Propylene Separation, PhD Thesis, Faculdade de Engenharia da Universidade do Porto, Porto, Portugal, 1999.

[21] Dantas, T. L. P., Luna, F. M. T., Silva Jr., I. J., Torres, A. E. B., de Azevedo, D. C. S., Rodrigues and A. E., Moreira, F. P. M., Modeling of the fixed-bed adsorption of carbon dioxide and a carbon dioxide-nitrogen mixture on zeolite 13X, *Brazilian Journal of Chemical Engineering*, 28, 533-544, 2011.

[22] Rios, R. B., Stragliotto, F. M., Peixoto, H. R., Torres, A. E. B., Bastos-Neto, M., Azevedo, D. C. S. and Cavalcante Jr., C. L., Studies on the behaviour of CO2-CH4 mixtures using activated carbon., *Brazilian Journal of Chemical Engineering*, 30, 939-951, 2013.

[23] Grande, C. A., Blom, R., Cryogenic Adsorption of Methane and Carbon Dioxide on Zeolites 4A and 13X, *Energy & Fuels*, 2014.

[24] Cavenati, S., Grande, C. A., Rodrigues, A. E., Adsorption Equilibrium of Methane, Carbon Dioxide, and Nitrogen on Zeolite 13X at High Pressures, *Journal of Chemical Engineering Data*, 49, 1095-1101, 2004.

[25] Cavenati, S., Grande, C. A., Rodrigues, A. E., Upgrade of Methane from Landfill Gas by Pressure Swing Adsorption, *Energy & Fuels*, 19, 2545-2555, 2005.

[26] Habgood, H. W., The kinetics of molecular sieve action. Sorption of nitrogen-methane mixtures by Linde molecular sieve 4A, *Canadian Journal of Chemistry*, 36, 1958.

[27] Gales, L., Mendes. A., and Costa, C., Hysteresis in the cyclic adsorption of acetone, ethanol and ethyl acetate on activated carbon, *Carbon*, 38, 1083-1088, 2000.

[28] Ferreira, D., Magalhães, R., Taveira, P. and Mendes, A., Effective Adsorption Equilibrium Isotherms and Breakthroughs of Water Vapor and Carbon Dioxide on Different Adsorbents, *Industrial & Engineering Chemistry Research*, 2011.